

1
2
3
4 1
5
6 2
7
8
9 3
10
11 4
12
13 5
14
15 6
16
17 7
18
19 8
20
21 9
22
23 10
24
25 11
26
27 12
28
29 13
30 14
31 15
32 16
33
34 17
35
36
37
38
39
40
41
42
43
44
45
46
47
48
49
50
51
52
53
54
55
56
57
58
59
60

Environments of tornadic and nontornadic supercells in China and optimized significant tornado parameter for China region

Ruqian Zhang¹, Ming Xue^{2*}, and Xiaoding Yu³

¹Key Laboratory of Mesoscale Severe Weather/Ministry of Education, School of Atmospheric Sciences, Nanjing University, Nanjing, Jiangsu 210023, China

²Center for Analysis and Prediction of Storms and School of Meteorology, University of Oklahoma, Norman, OK 73072, USA

³ China Meteorological Administration Training Center, Beijing 100081, China

Submitted December 9, 2024
Revised April 3, 2025

Corresponding author:
Ming Xue, mxue@ou.edu

Abstract

With a sample of 273 supercells spanning 20 years, inflow environment differences between tornadic and nontornadic supercells in China and its three subregions (northern, central and southern China; CNN, CNC, and CNS) are examined using sounding-derived parameters. Proximity soundings are extracted from the hourly ERA5 reanalysis data. The supercells are categorized as significantly tornadic [rated (E)F2+], weakly tornadic [rated (E)F1], and nontornadic. Thermodynamic parameters, such as convective available potential energy (CAPE), lifting condensation level (LCL), low-level relative humidity (RH) and convective inhibition (CIN), cannot discriminate between tornadic and nontornadic supercells effectively. In addition, thermodynamic parameters based on mixed-layer (ML) lifted parcels show worse skill than those for surface-based (SB) or most unstable (MU) lifted parcels. 0–300-m storm-relative helicity (SRH300) and 0–300-m bulk shear (SHR300) demonstrate greater forecasting skills compared to SRH and shear over deeper depths. Based on predictive skills and distributions of individual parameters, a new significant tornado parameter (STP) formulation, STP300cn, using MUCAPE, MULCL, MUCIN, SRH300, and SHR300 is composed. True Skill Score (TSS) is used to measure the capability of the individual or combined parameters in discriminating significantly tornadic from nontornadic supercells. The thresholds and normalization factors for terms in STP are calibrated to the China cases to obtain optimal predictive TSS scores. The calibrated STP parameter, called STP300cn, achieves a TSS of 0.51 in China overall, compared to the 0.14 and 0.29 of the two original versions of STP. It achieves a TSS of 0.37, 0.66, 0.42 for CNN, CNC and CNS, respectively, all much higher than those of the original STP parameters.

KEYWORDS

Supercells, new tornado parameter, storm environments, tornado forecasting

1. Introduction

Between 1961 and 2010, tornadoes in China caused at least 1,772 deaths and resulted in significant damage to property (Fan & Yu, 2015). Most intense tornadoes are associated with supercells but the majority of supercells (at least 70%) do not produce tornadoes (Coffer & Parker, 2015). Observational results have revealed remarkable similarities between tornadic and nontornadic supercells, including precipitation hook echoes, the presence of low-level mesocyclones (~1 km above ground level; AGL), occlusion downdrafts and updraft/downdraft structures spiraling cyclonically around the circulations (Lemon & Doswell, 1979; Trapp, 1999; Wakimoto & Cai, 2000; Wakimoto et al., 2004; Klees et al., 2016; Coffer & Parker, 2017).

Although tornadic and nontornadic supercells have many similarities, proximity soundings and numerical simulations have provided valuable insights into the environmental characteristics and possible mechanisms that distinguish them. Proximity soundings focus on thermodynamic and kinematic parameters such as convective available potential energy (CAPE), lifted condensation level (LCL), and vertical wind shear, examining the characteristics of pre-supercell environments (Weisman & Klemp, 1982; Brooks et al., 1994; Mead, 1997; Stensrud et al., 1997; Rasmussen & Blanchard, 1998; Thompson, 1998; Thompson et al., 2003). To better understand the relationship between environment parameters and tornado potential, it is useful to review the widely accepted three-step process of tornado formation within supercells: 1) Generation of a mid-level mesocyclone (approximately 3–7-km AGL); 2) Generation of surface vertical vorticity possibly via downdraft or updraft tilting of horizontal vorticity that is baroclinically or frictionally produced; and 3) Contraction of surface vertical vorticity into a tornado and sudden tilting of horizontal vorticity followed by intense stretching (Markowski & Richardson, 2014; Schenkman et al., 2014; Davies-Jones, 2015; Rotunno et al., 2017; Fischer & Dahl, 2022).

In the first step, the updraft, whose strength can be linked to CAPE (Klees et al., 2016), tilts and stretches horizontal vorticity associated with environmental wind shear to generate a mid-level mesocyclone. The mid-level mesocyclone largely results from horizontal streamwise vorticity in the environment (Davies-Jones, 1984). To forecast mesocyclone development, storm-relative helicity (SRH; Davies-Jones et al., 1990) over the inflow vertical range (typically 0–3-km) is preferred over streamwise vorticity because it is far less affected by measurement errors and sampling resolution and takes into account the storm-relative inflow speed (Davies-Jones, 2015). In addition to the 0–3-km SRH, Weisman and Klemp (1982, 1984, 1986) and Weisman (1996) emphasized the importance of strong vertical wind shear over substantial depths, specifically within the 0–4-km or 0–6-km layers. This is because the vertical dynamic pressure forcing needs to extend into the mid-levels of the troposphere to sustain updraft rotation. However, studies using proximity soundings have shown that SRH and vertical wind shear above 1 km are not noticeably different between tornadic and nontornadic supercells (e.g., Markowski et al., 1998, 2003; Thompson et al., 2003). Apart from observational studies, Coffer et al. (2017) using ensemble simulations found that both tornadic and nontornadic ensemble members contain storms with a strong mid-level updraft. In other words, the formation and intensity of the mid-level mesocyclone may not be the primary factor distinguishing between supercells that produce tornadoes and those that do not. The step 2 is not a sufficient condition for tornado formation either. Simulations by Coffer and Parker (2017) have shown that nontornadic supercells produced enough vertical vorticity in the step 2 but failed to stretch them due to disorganized low-level mesocyclones caused by the ingestion of mainly crosswise horizontal vorticity over the lowest few hundred meters AGL. In

1
2
3 94 contrast, tornadic supercells ingested mostly streamwise horizontal vorticity, leading to
4 95 a well-organized low-level mesocyclone that effectively enhanced vertical vorticity
5 96 stretching. Larger SRH over the lowest few hundred meters AGL can enhance the
6 97 development of a stronger low-level mesocyclone, resulting in more intense dynamic
7 98 lifting. This dynamic lifting may consequently stretch near surface vertical vorticity,
8 99 increasing the likelihood of tornadogenesis (Coffer & Parker, 2015; Coffer et al., 2017).
9
10 100 Building on this, Coffer et al. (2019) made improvements to the significant tornado
11 101 parameter (STP) in the United States using SRH over the 0–500-m layer AGL.
12 102 Additionally, Coffer et al. (2020) used SRH over the 0–100-m layer AGL to enhance
13 103 the predictability of STP in both the United States and Europe.

14
15 104 Combined parameters, including bulk Richardson number (BRN; Weisman &
16 105 Klemp, 1982), vorticity generation parameter (VGP; Rasmussen & Wilhelmson, 1983),
17 106 energy-helicity index (EHI; Hart & Korotky, 1991), supercell composite parameter
18 107 (SCP; Thompson et al., 2003) and STP (Thompson et al., 2003) incorporate both
19 108 kinematic and thermodynamic parameters. Among these combined parameters, STP is
20 109 one of the most widely used parameters for forecasting tornadic supercells. In addition
21 110 to 0–1-km SRH (SRH1) and 0–6-km wind shear (SHR6), the earlier version of STP
22 111 proposed by Thompson et al. (2003) also includes mixed-layer (ML, in the lowest 100
23 112 hpa) CAPE and MLLCL. Since 2005, the STP has been updated to use surface-based
24 113 (SB) parcels instead of ML parcels to calculate CAPE and LCL (Coffer et al., 2019).
25 114 The earlier STP can be called STP_{fix} for the fixed-layer calculation of kinematic terms.
26 115 To identify the layers that actually possess CAPE [without excessive values of
27 116 convective inhibition (CIN)] within the storm inflow, STP_{fix} is further adjusted to use
28 117 the effective storm inflow layer and effective storm depth for calculations of SRH and
29 118 bulk wind difference (ESRH and EBWD), respectively, resulting in the effective-layer
30 119 STP or STP_{eff} (Thompson et al., 2017). Additionally, the CIN term has been added to
31 120 STP_{eff} to reduce false alarms (Thompson et al., 2011). Thermodynamic terms in
32 121 STP_{eff} are calculated based on the height of ML. An STP value of 1 serves as a
33 122 reasonable guideline for distinguishing between significantly tornadic and nontornadic
34 123 supercells.

35
36
37
38 124 Studies indicate that tornado environments in China significantly differ from those
39 125 in the United States (Zhou et al., 2021; Zhang et al., 2023). In China, thermodynamic
40 126 conditions are generally conducive to tornado formation, characterized by moderate to
41 127 high CAPE and low to moderate LCL. In contrast, kinematic conditions in China are
42 128 notably less favorable compared to those observed in the United States (Zhang et al.,
43 129 2023). Therefore, we are interested in whether parameters such as STP still have
44 130 effective forecasting performance in China? Despite the importance of this question,
45 131 only a few studies have focused on the differences between tornado and non-tornado
46 132 storms and their environments in China. Zhou et al. (2012) analyzed several cases of
47 133 tornadic and nontornadic storms with mesocyclones and showed that tornadic
48 134 mesocyclones had larger values of mesocyclone excess rotational kinetic energy
49 135 (ERKE; Donaldson & Desrocher, 1990) and lower ERKE-weighted mesocyclone
50 136 height than nontornadic ones. Yu et al. (2021) compared environmental parameters
51 137 characterizing tornadic and nontornadic supercells in China from 2002–2016 using
52 138 neighboring soundings and surface observations. They found that SHR6 and CAPE
53 139 could not discriminate tornadic from nontornadic supercells, while 0–1-km shear and
54 140 LCL were somewhat able to do so. Their studies did not examine environmental
55 141 parameters comprehensively nor assess the ability of STP to distinguish between
56 142 tornado and non-tornado events. The limited availability of neighboring soundings at

1
2
3 143 times close to tornado events also affected the generality of conclusions obtained in that
4 144 study.

5 145 This paper utilizes the fifth-generation European Centre for Medium-Range
6 146 Weather Forecasting (ECMWF) reanalysis (ERA5; Hersbach et al., 2020) that has
7 147 higher spatial and temporal resolutions compared to other global reanalysis datasets to
8 148 extract proximity soundings and calculate environmental parameters. With 20-year
9 149 samples (2002-2021) of tornado and non-tornado supercells, this study aims to identify
10 150 inflow environment differences between tornadic and nontornadic supercells using
11 151 sounding-derived parameters and to enhance the predictability of STP in China. Given
12 152 that recent studies have demonstrated that low-level wind shear exhibits considerable
13 153 skill in predicting tornadoes (Brooks et al., 2003; Markowski et al., 2003; Coffey &
14 154 Parker, 2015, 2017, 2018; Coffey et al., 2019, 2020), this study also explores whether
15 155 using vertical wind shear in a shallower layer can improve the predictive skill of STP
16 156 for tornadic supercell cases from China. In particular, this study tries to answer the
17 157 following questions:

- 18 158 1) What are the environmental characteristics of tornadic and nontornadic
19 159 supercells in China?
- 20 160 2) How skillful are the two forms of STP (STPfix and STPeff) in predicting
21 161 tornadoes in China?
- 22 162 3) Can SRH over a shallower layer achieve a greater ability in differentiating
23 163 between tornadic and nontornadic supercells in China, similar to findings in
24 164 America and Europe (Coffey et al., 2019, 2020)?
- 25 165 4) Does shallow-layer vertical wind shear exhibit comparable forecasting skill to
26 166 shallow-layer SRH?

27 167 The rest of this paper is organized as follows. Section 2 describes the methods used
28 168 in the study, along with the data and regions in detail. Section 3 presents the
29 169 environmental characteristics of tornadic and nontornadic supercells. Improvements to
30 170 the STP in China are illustrated in section 4. Discussion and conclusions about the study
31 171 are given in sections 5 and 6.

32 172 **2. Data and methods**

33 173 The 2002-2021 dataset of tornado and non-tornado cases used in this study comes
34 174 from four sources. The primary sources are the “Collection of Meteorological Disasters
35 175 Records in China” (Ding, 2008) and the “Yearbook of Meteorological Disasters in
36 176 China” (China Meteorological Administration, 2005–2022). Information from
37 177 meteorological bureaus in China and online sources are also utilized. Furthermore,
38 178 Doppler radar data are used to confirm that all cases are of the supercell type based on
39 179 the characteristics of mesocyclone and reflectivity pattern. (E)F0 tornadoes cause
40 180 minimal damage and are difficult to document comprehensively. Therefore, this study
41 181 excludes tornadic supercells rated (E)F0. Tornadoes are generally categorized into two
42 182 types: typical tornadoes and tropical cyclone (TC) tornadoes (less frequent). The
43 183 environment within TC tornadoes is characterized by higher deep-layer humidity and
44 184 lower CAPE (Edwards et al., 2012), setting it apart from the environment of typical
45 185 tornadoes. As a result, TC tornadoes (account for about 10% of total cases examined)
46 186 are excluded in this paper. Nontornadic supercells associated with TC environments are
47 187 also excluded. Supercells in this paper are categorized as significantly tornadic [sigtor,
48 188 rated (E)F2 or greater, 57 cases], weakly tornadic [weaktor, rated (E)F1, 73 cases], and
49 189 nontornadic [nontor, 159 cases]. Most nontornadic cases collected exhibit severe
50 190 intensity, characterized by hail larger than 4 mm, strong wind exceeding 20 m/s, or
51 191 short-term heavy rainfall. Due to limitations in data records (which are inherently

192 limited and not all examples have precise timestamps or locations) and the distribution
 193 of Doppler radar stations in China, the number of non-tornado cases is not significantly
 194 greater than that of tornadic cases. However, it is beneficial to have at least comparable
 195 sample sizes of tornadic and nontornadic supercells.

196
 197 Table 1. The number and percentage of significantly tornadic supercells
 198 (sigtor), weakly tornadic supercells (weaktor) and nontornadic
 199 supercells (nontor) for northern (CNN), central (CNC), and southern
 200 China (CNS).

	CNN		CNC		CNS	
	number	percentage	number	percentage	number	percentage
sigtor	22	21%	28	29%	7	10%
weaktor	25	24%	18	19%	30	42%
nontor	58	55%	51	53%	34	48%

201
 202 Only a few tornadic and nontornadic cases are observed in the western regions, such
 203 as Xinjiang province (XJ; Figure 1). Tornadic cases are primarily concentrated in the
 204 eastern regions of China, while nontornadic cases are more widely distributed. In
 205 addition to their prevalence in eastern China, nontornadic cases that we collected also
 206 extend into topographically complex regions such as Guizhou province (GZ). To
 207 exclude the influence of terrain on the environmental differences between tornadoes
 208 and non-tornadoes, the 16 non-tornado examples from Guizhou, Yunnan, Sichuan,
 209 Chongqing and Qinghai provinces (GZ, YN, SC, CQ, and QH) are excluded from the
 210 subsequent analysis. Moreover, to assess the predictive performance of sounding-
 211 derived parameters in various regions of China, following Zhang et al. (2023), we
 212 further divide China into northern (CNN), central (CNC) and southern China (CNS)
 213 using latitude lines 35°N and 27.5°N (Figure 1a). The percentages of the three storm
 214 types are similar in the CNN and CNC regions, while the number of significant tornado
 215 cases we collected is lowest in the CNS region (Table 1). The monthly distribution of
 216 each storm type has greater variability than the diurnal distribution (Figure 2). Tornadic
 217 supercells are more frequent in summer, with a peak occurrence in July, while
 218 nontornadic supercells tend to occur in spring, peaking in April with a secondary peak
 219 in June. Tornadic and nontornadic supercells exhibit some similarities in their daily
 220 distributions, with both being more prevalent in the late afternoon. This overlap makes
 221 it more challenging to distinguish them. The collected examples of tornadic and
 222 nontornadic supercells do not exhibit a high degree of spatial and temporal overlap,
 223 which may lead to inaccurate statistical results. However, since our focus is on the
 224 surrounding environment of supercells themselves, with the high-resolution ERA5 data
 225 and the proximity sounding calculation method we used, this study could still provide
 226 valuable insights into distinguishing tornadic and nontornadic supercells in China.

1
2
3
4
5
6
7
8
9
10
11
12
13
14
15
16
17
18
19
20
21
22
23
24
25
26
27
28
29
30
31
32
33
34
35
36
37
38
39
40
41
42
43
44
45
46
47
48
49
50
51
52
53
54
55
56
57
58
59
60

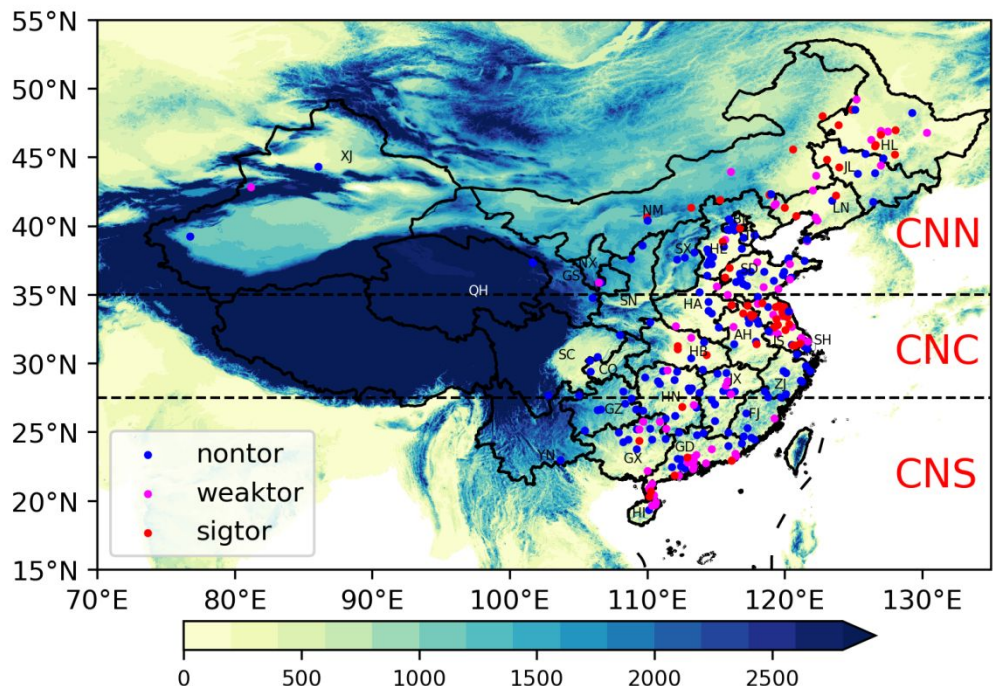


Figure 1. Maps of the regional distribution of significantly tornadic supercells (sigtor), weakly tornadic supercells (weaktor), and nontornadic supercells (nontor) in northern (CNN), central (CNC), and southern China (CNS). The two black dashed lines represent 35°N and 27.5°N latitude line respectively.

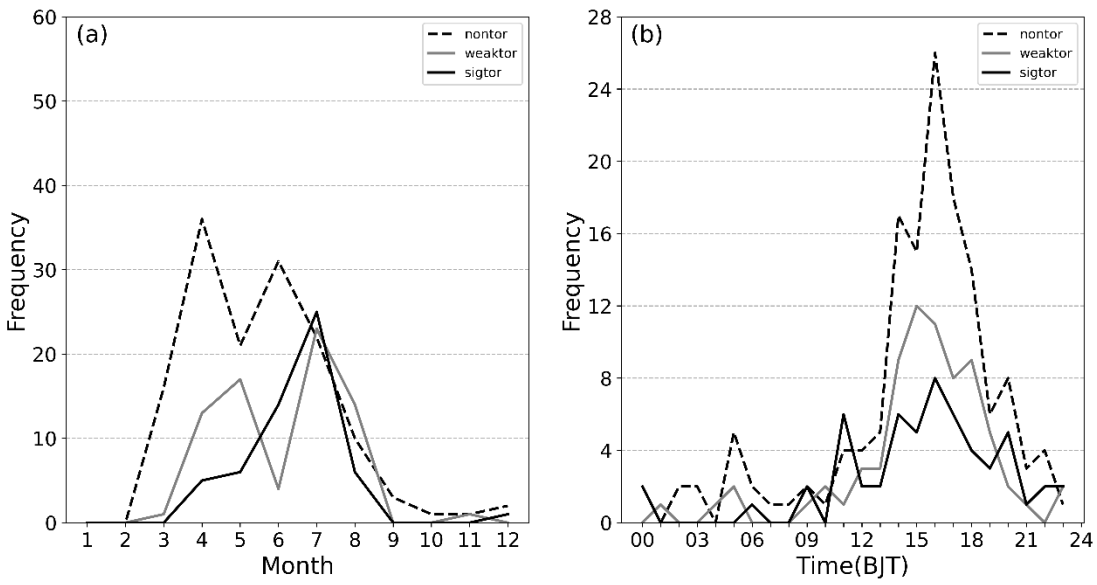


Figure 2. Monthly variations (a) and diurnal variations (b) of significantly tornadic supercells (sigtor), weakly tornadic supercells (weaktor), and nontornadic supercells (nontor) in China

The use of proximity soundings to discern the characteristics of thunderstorms dates back to the 1940s (Showalter & Fulks, 1943; Fawbush & Miller, 1954; Beebe, 1958). These early investigations were conducted using relatively sparse observed soundings. Later, proximity soundings derived from 3- or 6-hourly radiosonde observations and

244 model analyses were used to explore pre-storm environments (Mead, 1997; Rasmussen
 245 & Blanchard, 1998; Thompson, 1998; Evans & Doswell, 2001; Craven & Brooks,
 246 2004). However, due to the often large deviation of the data time from the actual start
 247 time of tornadoes, these methods may be less reliable. Recently, hourly ERA5
 248 reanalysis data with higher resolution has been applied to such studies (Coffer et al.,
 249 2020; Taszarek et al., 2020; Veloso-Aguila et al., 2023; Zhang et al., 2023). Proximity
 250 soundings used in this paper are extracted from the ERA5 reanalysis dataset, which has
 251 a horizontal spatial resolution of 0.25° and 37 pressure levels in the vertical. While the
 252 ERA5 data in the native hybrid sigma-isentropic coordinates offer higher vertical
 253 resolution near the ground, that data is harder to download and process. Although the
 254 pressure level data are not ideal for calculating shallow-layer SRH and shear, the
 255 calculated parameters still show notable predictive skills, as discussed in section 4b.

256 The proximity-inflow method employed in this study is described in Zhang et al.
 257 (2023) and follows the original procedure of Rasmussen and Blanchard (1998). With
 258 this method, soundings extracted from the ERA5 are used to represent the inflow
 259 environments of the supercell storm events. The sounding corresponding to each event
 260 features the closest hourly time before the event. It is within a 100 km radius of the
 261 event location and falls within $\pm 75^\circ$ of the inflow wind vector. More details can be
 262 found in Zhang et al. (2023). The sounding-derived parameters are calculated based on
 263 the Sounding and Hodograph Analysis and Research Program in Python (SHARPPy),
 264 an open-source, cross-platform, upper-air sounding analysis and visualization package
 265 (Blumberg et al., 2017). Almost all routines in SHARPPy are written to be as consistent
 266 as possible with the methods used at the U.S. National Weather Service (NWS) Storm
 267 Prediction Center (SPC).

268 As mentioned above, STP, which performs well in distinguishing significantly
 269 tornadic and nontornadic supercells in the United States, upgrades from the fixed
 270 version to the effective version with respect to the depth over which SRH and BWD
 271 are calculated. The formulations of the two versions are

$$272 \text{STP}_{\text{fix}} = \left(\frac{\text{SBCAPE}}{1500 \text{ J kg}^{-1}} \right) \times \left(\frac{2000 - \text{SBLCL}}{1000 \text{ m}} \right) \times \left(\frac{\text{SRH1}}{150 \text{ m}^2 \text{ s}^{-2}} \right) \times \left(\frac{\text{BWD6}}{20 \text{ m s}^{-1}} \right) (1)$$

$$273 \text{STP}_{\text{eff}} = \left(\frac{\text{MLCAPE}}{1500 \text{ J kg}^{-1}} \right) \times \left(\frac{\text{MLCIN} + 200}{150 \text{ J kg}^{-1}} \right) \times \left(\frac{2000 - \text{MLLCL}}{1000 \text{ m}} \right) \times \left(\frac{\text{ESRH}}{150 \text{ m}^2 \text{ s}^{-2}} \right) \times \left(\frac{\text{EBWD}}{20 \text{ m s}^{-1}} \right). (2)$$

274 In formulation (1), the SBLCL term is assigned a value of 0.0 when SBLCL exceeds
 275 2000 m, and assigned a value of 1.0 when SBLCL is less than 1000 m. The BWD6 here
 276 is the 0–6-km vertical wind shear (Klees et al., 2016). The BWD6 term is set to 0.0
 277 when BWD6 is less than 12.5 m s^{-1} and set to 1.0 when BWD6 is greater than 30 m s^{-1} .
 278 In formulation (2), modifications involve the addition of the MLCIN term and a change
 279 in the calculation depth of SRH and BWD parameters, while other aspects remain
 280 unaltered. The MLCIN term is assigned a value of 0.0 when MLCIN is less than -150 J
 281 kg^{-1} and set to 1.0 when MLCIN exceeds -50 J kg^{-1} .

282 Significant tornadoes have a high potential for destruction, and this study focuses
 283 on evaluating the ability of various parameters to forecast such events. The forecast
 284 verification of parameters is through the traditional 2×2 contingency table (Doswell
 285 & Flueck, 1989; Doswell et al., 1990) and its associated skill measures. As in
 286 Thompson et al. (2003), the true skill statistics (TSS), which is also commonly referred
 287 to as the Pierce skill score (Pierce, 1884), is used to identify the environmental
 288 parameters which are effective in distinguishing between significantly tornadic and
 289 nontornadic supercells. TSS is equal to

$$\text{TSS} = \frac{(ad - bc)}{(a + c)(b + d)}, (3)$$

where a denotes correct forecasts of the event, b denotes wrong forecasts of the nonevent, c represents wrong forecasts of the event and d represents correct forecasts of the nonevent. The TSS can be interpreted as the disparity between two conditional probabilities in the likelihood-base rate factorization of the joint distribution, namely, the hit rate (POD) and the false alarm rate (POFD; Wilks, 2020). Perfect forecasts are assigned a TSS value of one, random forecasts receive a TSS value of zero and forecasts inferior to the random forecasts get negative scores.

3. Environmental characteristics

a. Thermodynamic parameters

In the United States, both MLCAPE and MLLCL values show a monotonic relationship among storm groups (e.g., significantly tornadic cases have the highest MLCAPE, weakly tornadic cases show intermediate MLCAPE values, nontornadic cases have the lowest MLCAPE) and when comparing significantly tornadic and nontornadic supercells, they are proven to be operationally useful (Thompson et al., 2003). In contrast, thermodynamic parameters based on ML lifted parcels exhibit low predictive capability for tornadoes in China (Figure 3). This may be one reason why the original STPeff (discussed in more detail below) shows poor forecasting skills in China.

Table 2. The maximum TSS and the optimal threshold for specific forecasting parameters differentiate significantly tornadic supercells from nontornadic supercells in China. TSS is computed across 1000 evenly distributed thresholds of the entire ERA5 sounding dataset for each variable.

	Max TSS	Optimal threshold
MLCAPE	0.06	1698.1
SBCAPE	0.18	2858.1
MUCAPE	0.18	2859.1
MLLCL	0.19	1350.2
SBLCL	0.29	828.2
MULCL	0.29	827.4
MLCIN	0.10	-109.3
SBCIN	0.10	-19.2
MUCIN	0.05	-107.5
lowRH	0.15	75.3
LR85	0.01	8.2
LR75	0.02	8.0
ESRH	0.29	75.7
SRH1	0.34	58.8
SRH300	0.48	10.4
SHR6	0.06	30.0

EBWD	0.01	31.8
SHR300	0.48	2.3
EHI	0.26	0.9
VGP	0.17	0.2
BRN	0.07	31.6
SCP	0.18	11.5
STPfix	0.29	0.5
STPeff	0.14	0.7
STP300cn	0.51	1.0

314

315 MLCAPE values for significantly tornadic and nontornadic supercells differ by
 316 nearly one quartile between the 25th and the 75th percentiles of each distribution in the
 317 United States (Thompson et al., 2003). However, MLCAPE values for most
 318 significantly tornadic cases are lower than those for nontornadic cases in China (Figure
 319 3a). Yu et al. (2021) also found that the distribution intervals of MLCAPE values for
 320 tornadic and nontornadic supercells in China are highly overlapping. Hence, MLCAPE
 321 is not a good predictor for tornadic supercells in China ($TSS_{MLCAPE}=0.06$; Table 2).
 322 Additionally, parameters derived from the SB and the most unstable (MU, in the lowest
 323 300 hpa) layers are examined. The boxplot of SBCAPE closely mirrors that of
 324 MUCAPE, with one slight contrast: the 25th to 75th percentile rank values of MUCAPE
 325 for significantly tornadic supercells consistently surpass those for nontornadic
 326 supercells, but it is not so for SBCAPE (Figures 3d and 3g). From MLCAPE to
 327 SBCAPE or MUCAPE, TSS increases from 0.06 to 0.18 (Table 2).

328 Lower LCL indicates higher relative humidity (RH), potentially leading to
 329 enhanced buoyancy in the rear-flank downdraft or inflow and an elevated likelihood of
 330 tornado formation (Markowski et al., 2002). MLLCL in China has similar
 331 characteristics between significantly tornadic and nontornadic supercells (Figure 3b).
 332 In contrast, the percentile-ranked values of MLLCL in the United States demonstrate a
 333 great difference (more than one quartile) between significantly tornadic and
 334 nontornadic supercells (Thompson et al., 2003). MLLCL in China seems to lack any
 335 correlation with the storm types. The TSS value of MLLCL is 0.19 (Table 2), which is
 336 greater than the TSS value of MLCAPE. Besides, the median value of MULCL for
 337 tornadic supercells is moderately lower compared to that of nontornadic supercells
 338 (Figure 3e). SBLCL has a similar distribution to MULCL (Figures 3e and 3h). Both
 339 SBLCL and MULCL achieve a TSS value of 0.29 (Table 2).

340 Supercells producing significant tornadoes tend to have less CIN than nontornadic
 341 supercells (Rasmussen & Blanchard, 1998; Davies, 2004). The physical explanation is
 342 that large CIN may inhibit the ascent and stretching of low-level parcels, reducing the
 343 probability of tornadoes (Davies, 2004). However, CIN is not useful either in
 344 distinguishing tornadic and nontornadic supercells in China. The TSS value of CIN is
 345 always around 0.1 regardless of the calculation depth (Table 2). As shown in Figures
 346 3c, 3f, and 3i (displaying absolute CIN values), the boxplots of CIN for significantly
 347 tornadic supercells largely overlap with those for nontornadic supercells, and weakly
 348 tornadic supercells have the lowest median of CIN. The median CIN for nontornadic
 349 supercells in China is lower than that in the United States (Davies, 2004). Absolute

350 Values larger than 50 J kg^{-1} can be viewed as large CIN. In China, only about 25% of
 351 nontornadic supercells occur with CIN larger than 50 J kg^{-1} (Figures 3c, 3f and 3i).
 352 These characteristics of CIN may explain its limited forecasting ability in China.

353
 354

Table 3. As in Table 2, but for the regions divided in Figure 1.

	CNN		CNC		CNS	
	Max	Optimal	Max	Optimal	Max	Optimal
	TSS	threshold	TSS	threshold	TSS	threshold
MLCAPE	0.07	2703.8	0.17	1433.6	0.25	1386.4
SBCAPE	0.05	60.3	0.27	3206.1	0.28	2742.6
MUCAPE	0.02	3771.4	0.28	2264.7	0.28	2740.9
MLLCL	0.25	1278.7	0.35	1186.7	0.10	828.1
SBLCL	0.22	919.0	0.54	697.6	0.13	345.8
MULCL	0.24	990.6	0.54	824.6	0.19	347.0
MLCIN	0.16	-88.2	0.08	-17.1	0.32	-41.0
SBCIN	0.13	-88.6	0.15	-20.5	0.27	-31.8
MUCIN	0.12	-98.2	0.15	-20.6	0.21	-31.7
SRH1	0.40	54.4	0.50	52.7	0.25	138.0
ESRH	0.37	75.8	0.40	69.4	0.08	146.5
SRH300	0.51	13.0	0.63	24.4	0.25	19.1
SHR6	0.16	15.0	0.06	15.6	0.14	33.1
EBWD	0.12	19.0	0.05	10.8	0.02	27.0
SHR300	0.50	2.3	0.57	3.4	0.42	1.1
STPfix	0.27	0.4	0.51	0.5	0.08	2.5
STPeff	0.06	1.3	0.38	0.5	0.00	0.0
STP300cn	0.37	1.4	0.66	1.3	0.42	1.0

355
 356

357 The forecast skill of thermodynamic parameters varies regionally. One notable fact
 358 is that, across three regions, thermodynamic parameters in CNN typically score lower
 359 values (Table 3). With TSS values hovering around 0.1 (Table 3), CAPE proves to be
 360 the least effective parameter in the CNN region. The cold vortex serves as the primary
 361 synoptic background for tornadoes in CNN (Zheng, 2020). Tornadoes occurring under
 362 this environment typically exhibit lower CAPE values, a result of reduced low-level
 363 moisture and a shallower moist layer (Wang et al., 2015). The poor performance of
 364 thermodynamic parameters in the CNN region may be attributed to the characteristics
 365 of supercells within cold vortices, which tend to have lower CAPE, drier conditions,
 366 and larger CIN, making it difficult to distinguish between tornadic and nontornadic
 367 supercells (Table 3). For tornadoes in the CNN region, kinematic parameters play more
 368 important roles, which will be discussed further later. Thermodynamic parameters
 369 generally perform better in the CNS region, with the exception of LCL, which has a
 370 lower TSS value of ~ 0.1 – 0.2 compared to the CNC region (Table 3). The poor
 371 performance of LCL is attributed to the overall humid environment in the CNS region,
 372 resulting in similarly low LCL values for both tornadic and nontornadic supercells. In

373 contrast, CAPE and CIN achieve better scores in the CNS region (Table 3), indicating
 374 that the tornado in this region does benefit from favorable environmental
 375 thermodynamic conditions. Supercells located in CNC are not constrained by regional
 376 humidity and achieve the highest LCL scores (~0.4-0.5; Table 3). Associated with
 377 relatively high TSS values of CAPE and CIN (Table 3), significant tornadoes benefit
 378 most from favorable thermodynamic condition in the CNC region, likely due to the
 379 larger variability in environmental humidity and temperature conditions in the region.
 380 Besides, thermodynamic parameters based on SB or MU lifted parcels both perform
 381 better than ML lifted parcels in the CNC region (Table 3).

382

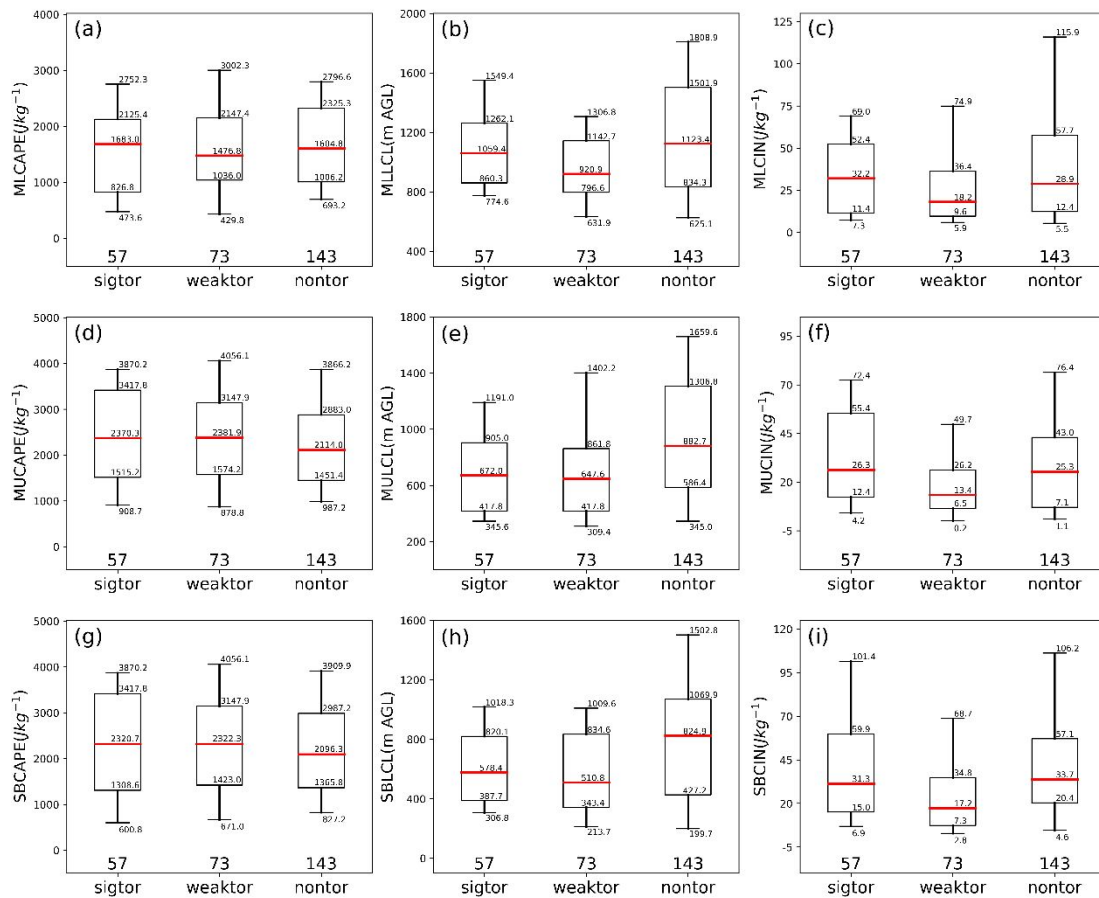


Figure 3. Box-and-whisker plots of (a) MLCAPE, (b) MLLCL, (c) the absolute values of MLCIN, (d) MUCAPE, (e) MULCL, (f) the absolute values of MUCIN, (g) SBCAPE, (h) SBLCL, and (i) the absolute values of SBCIN for significantly tornadic supercells (sigtor), weakly tornadic supercells (weaktor), and nontornadic supercells (nontor). The median value for each category is represented by a red line within the box. The boxes span the 25th–75th percentiles and the whiskers extend to the 10th and 90th percentiles. The numbers of cases for each group are listed below the columns.

Figure 4 shows the composite soundings of significantly tornadic, weakly tornadic, and nontornadic supercells. To avoid the over-smoothing effect, the soundings in Figure 4 employ the realignment method described in subsection 3b. In China, the low-level environments are warm for all three storm types due to their similar diurnal variance, wetter for weakly tornadic supercells, and drier for both significantly tornadic

1
2
3 400 and nontornadic supercells (Figure 4). Low-level RH could not distinguish significantly
4 401 tornadic and nontornadic clearly (i.e., $TSS_{lowRH} = 0.15$; Table 2). Unlike low-level RH,
5 402 mid-to-high-level RH is clearly higher in tornadic supercells compared to nontornadic
6 403 supercells (Figure 4). The positive CAPE areas on the skew T diagram of different
7 404 storm types are similar, albeit with a slightly higher average value of CAPE for
8 405 nontornadic supercells (Figure 4). Besides, other thermodynamic parameters including
9 406 850-500hPa lapse rate (LR85), 700-500hPa lapse rate (LR75), and level of free
10 407 convection (LFC) show limited ability to forecast tornadoes. This is supported by the
11 408 average values of these parameters shown in Figure 4, which either demonstrate
12 409 similarities or lack a monotonic relationship among storm groups.

13
14
15 410 Clearly, thermodynamic parameters perform poorly in predicting tornadoes in
16 411 China. However, shallow-layer SRH and shallow-layer shear could potentially serve as
17 412 effective discriminators between tornadic and nontornadic supercells. We will discuss
18 413 this in the next subsection.
19 414

20
21
22
23
24
25
26
27
28
29
30
31
32
33
34
35
36
37
38
39
40
41
42
43
44
45
46
47
48
49
50
51
52
53
54
55
56
57
58
59
60

For Peer Review

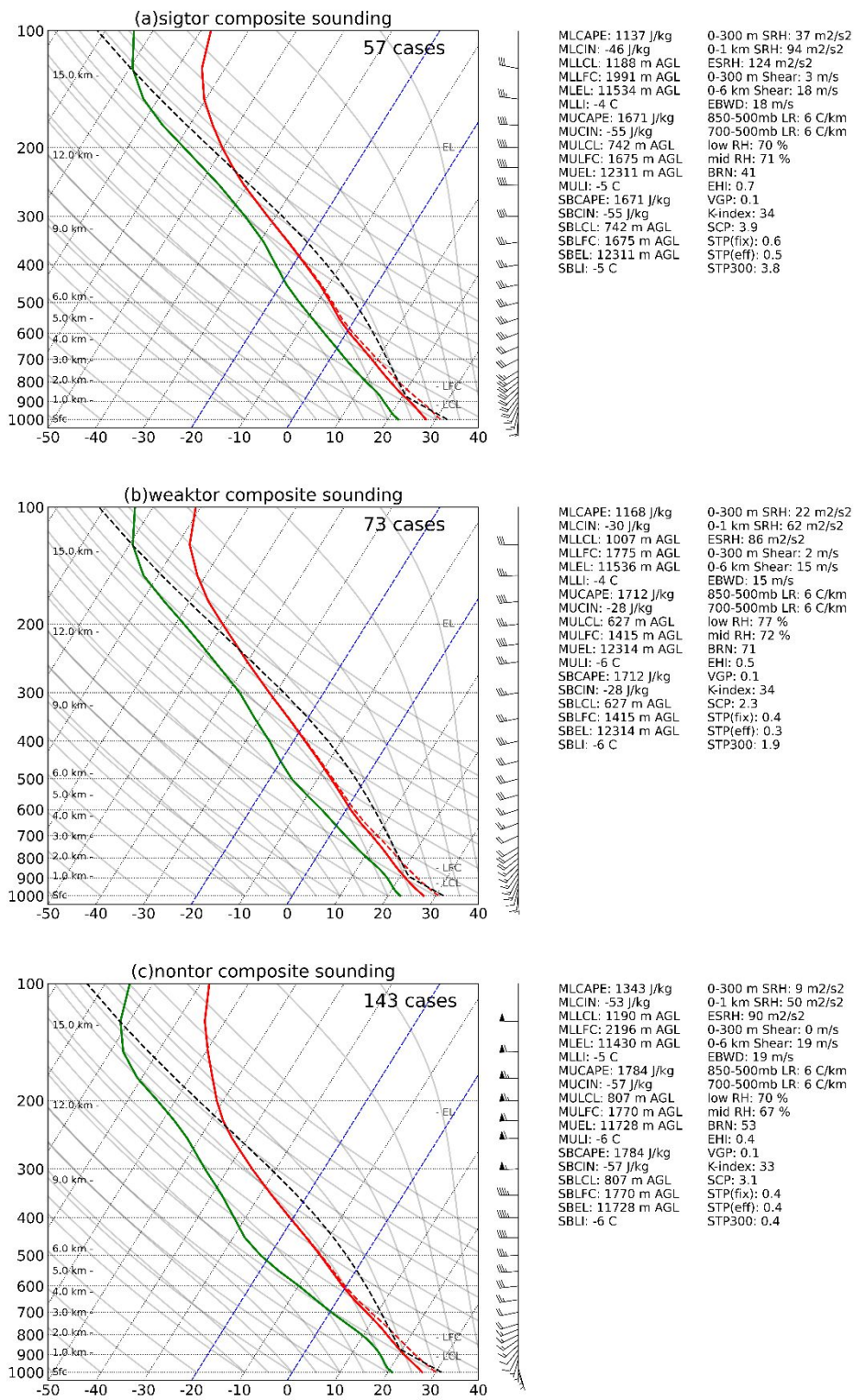


Figure 4. Composite soundings of (a) significantly tornadic supercells (sigtor; 57 cases), (b) weakly tornadic supercells (weaktor; 73 cases), and (c) nontornadic supercells (nontor; 143 cases). Solid red, solid green, dashed red and dashed black lines denote temperature, dewpoint, virtual temperature, and parcel trace. Dashed blue lines denote 0°C and -20 °C isotherms. The composite wind profile for each region is the average of individual wind profiles after their 0–6-km shear vector is aligned with the mean 0–6-km shear vector. Mean values of different parameters are shown on the right.

1
2
3 426 *b. Kinematic parameters*
4

5 427 In China, the median of 0–1-km AGL SRH (SRH1) for significantly tornadic
6 428 supercells is almost 2.5 times larger than that for nontornadic supercells (Figure 5b).
7 429 The median of ESRH for significantly tornadic is 1.5 times larger than that for
8 430 nontornadic supercells (Figure 5c). Additionally, ESRH does not exhibit a monotonic
9 431 relationship across storm groups. In other words, the distribution of ESRH for weakly
10 432 tornadic supercells is similar to that for nontornadic supercells (Figure 5c). Therefore,
11 433 SRH1 has better forecast skill than ESRH. About 95% of supercells in this study are
12 434 surface-based (i.e., the bottom height of effective inflow is zero) and the median depth
13 435 of the effective inflow layer is about 1929 m, which is deeper than the depth of SRH1.
14 436 A shallower layer of SRH may have a greater performance (e.g., SRH1 performs better
15 437 than ESRH). As shown in Figure 5a, 0–300-m AGL SRH (SRH300) has the best
16 438 predictive ability among SRH over other layer depths. The 25th percentile of SRH300
17 439 for significantly tornadic supercells roughly matches the 75th percentile of SRH300 for
18 440 nontornadic supercells (Figure 5a). Evidently, SRH300 gets a high TSS value of 0.48
19 441 (Table 2). SRH1 follows SRH300 with a lower TSS (0.34; Table 2), while ESRH
20 442 achieves the lowest score (0.29; Table 2). Compared to the deeper layers used
21 443 traditionally in operations, increasingly shallower layers of SRH result in increased
22 444 forecast skill. Variances also exist across different regions in China. CNC, which has
23 445 the largest number of significantly tornadic cases, consistently demonstrates superior
24 446 SRH forecasting ability, regardless of the calculation depth of SRH (Table 3). Next
25 447 to CNC in terms of SRH performance is CNN, with a score difference of only around
26 448 0.1 (Table 3). This further suggests that kinematic environmental conditions have more
27 449 effect on significant tornadoes in CNN. Consistently, SRH300 scores highest compared
28 450 to other depths of SRH in these two regions. However, SRH performs worse in the CNS
29 451 region, with ESRH achieving the lowest TSS value of 0.08 (Table 3). The lower SRH
30 452 scores in CNS, compared to other regions, can be attributed to the relatively low
31 453 horizontal streamwise vorticity in the region's environment. This is also a key factor
32 454 contributing to the lowest proportion of significant tornadoes (excluding TC tornadoes)
33 455 in CNS, as shown in Table 1.

34 456 In China, the vertical wind shear over a deeper depth (SHR6 and EBWD) also
35 457 shows poor forecasting skills. The median values of SHR6 and EBWD for significantly
36 458 tornadic supercells are slightly lower than those for nontornadic supercells (Figures 5e
37 459 and 5f), consistent with the findings of Yu et al. (2021), who observed similar SHR6
38 460 distributions in China. Switching from a fixed-layer to an effective-layer calculation of
39 461 deep shear does not enhance tornado forecasting performance ($TSS_{SHR6} = 0.06$,
40 462 $TSS_{EBWD} = 0.01$; Table 2). SHR6 and EBWD can discriminate between supercells and
41 463 nonsupercells, but not tornadic and nontornadic supercells (Thompson et al., 2003,
42 464 2007). In contrast, the median of 0–300-m AGL bulk shear (SHR300) for significantly
43 465 tornadic supercells is almost four times higher than that for nontornadic supercells
44 466 (Figure 5d). In line with this, the TSS value of SHR300 is significantly higher
45 467 ($TSS_{SHR300} = 0.48$; Table 2). Low-level shear contributes to strengthening, widening,
46 468 and lowering of the base of the mesocyclone, inducing stronger dynamic lifting that
47 469 could forcibly lift low-level flow with appreciable vorticity (Coffer & Parker, 2015).
48 470 This study further demonstrates that shallow-layer shear has a great ability to forecast
49 471 tornadic supercells, as does shallow-layer SRH. The variance of bulk shear across
50 472 geographic regions is similar to that of SRH. The CNC region often experiences varying
51 473 weather systems from the north and south, and prior to strong northwesterly upper-level
52 474 flows overlaying strong low-level southerly flows, resulting in great wind shear
53 475 conditions. Specifically, for SHR300, CNC achieves the highest value of 0.57, while

476 CNN and CNS attain values of 0.50 and 0.42, respectively (Table 3). For significant
 477 tornadoes in the CNS region, wind shear proves to be a more effective parameter
 478 compared to SRH. Additionally, the TSS values for kinematic parameters in the CNS
 479 region are lower than those observed in other regions. This discrepancy may be
 480 attributed to the relatively weak wind shear environment in the CNS region.
 481 Nevertheless, SHR300 remains the most effective differentiator among individual
 482 kinematic and thermodynamic parameters in CNS.

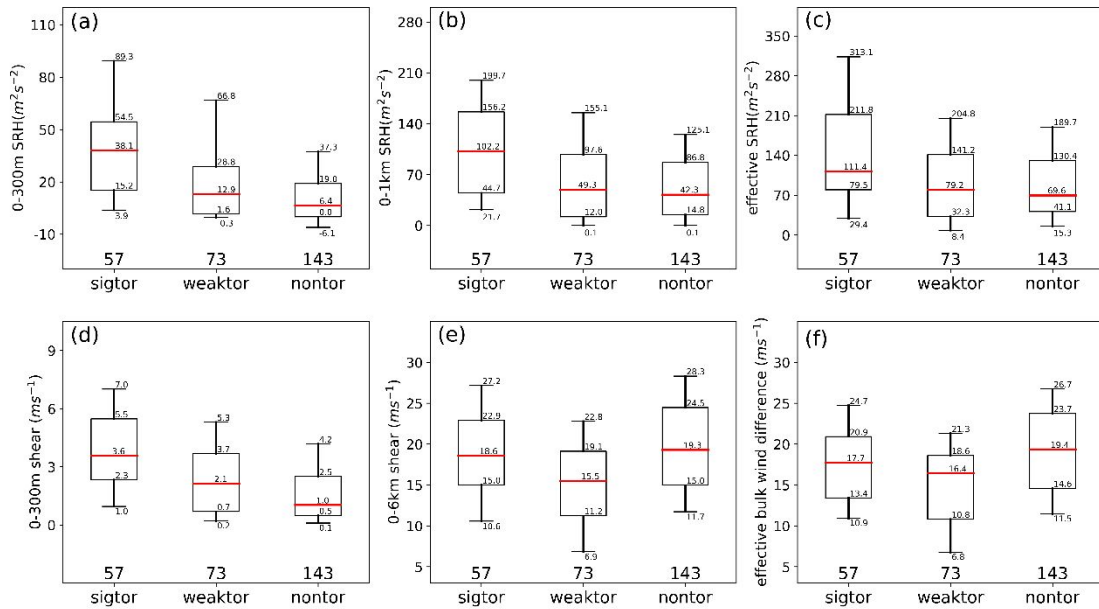


Figure 5. Box-and-whisker plots of (a) SRH300, (b) SRH1, (c) ESRH, (d) SHR300, (e) SHR6, and (f) EBWD for significantly tornadic supercells (sigtor), weakly tornadic supercells (weaktor), and nontornadic supercells (nontor). Other descriptions are as in Figure 3.

490 To explore the vertical wind shear characteristics among different types of storms,
 491 composite hodographs are presented in Figure 6. To prevent over-smoothing from
 492 obscuring the original characteristics of the 0–6-km wind shear vector, which may
 493 exhibit varying orientations, this paper employs the same realignment method as Zhang
 494 et al. (2023). The dashed black curve in each panel denotes the composite hodograph
 495 without realignment, while solid red represents the composite hodograph after all
 496 individual hodographs are first realigned based on 0–6-km shear before averaging. The
 497 dashed black and the solid red of the hodograph for each storm type are quite similar,
 498 indicating that most cases have similar 0-6 km shear orientations (Figure 6). The low-
 499 level shear in three composite hodographs all exhibits clockwise rotation, with
 500 significantly tornadic supercells showing the largest curvature (Figure 6). In particular,
 501 accompanied by a notable increase in the southerly component, the composite
 502 hodograph of significantly tornadic supercells from 0 to 300 m has a corresponding
 503 increase (Figure 6a). In sharp contrast, the composite hodograph of nontornadic cases
 504 from 0 m to 300 m remains nearly constant (Figure 6c). Besides, unlike the nearly
 505 identical shapes of composite hodographs at higher levels in the United States (Coffer
 506 et al., 2020), the shapes of tornadic and nontornadic hodographs above 6 km in China
 507 are different (Figure 6). The hodograph of nontornadic supercells above 6 km displays
 508 a significant increase in the westerly component. This may be attributed to the
 509 relatively strong supercell intensity of the non-tornado cases collected in this paper.
 510

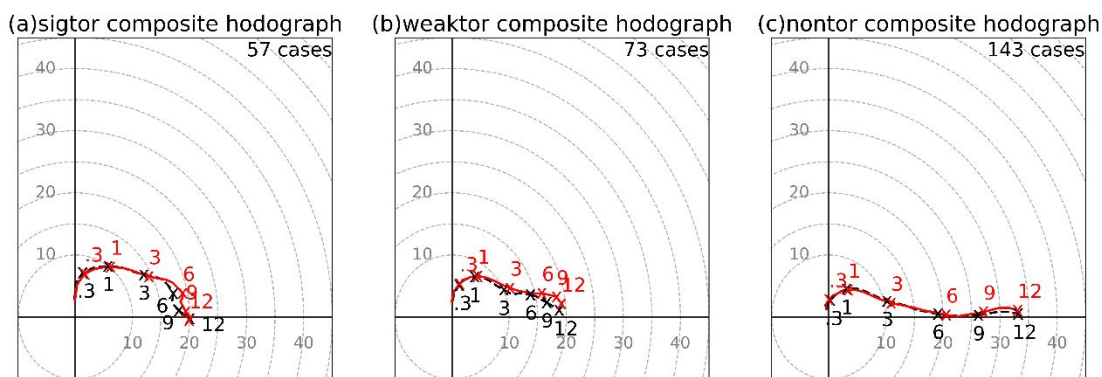
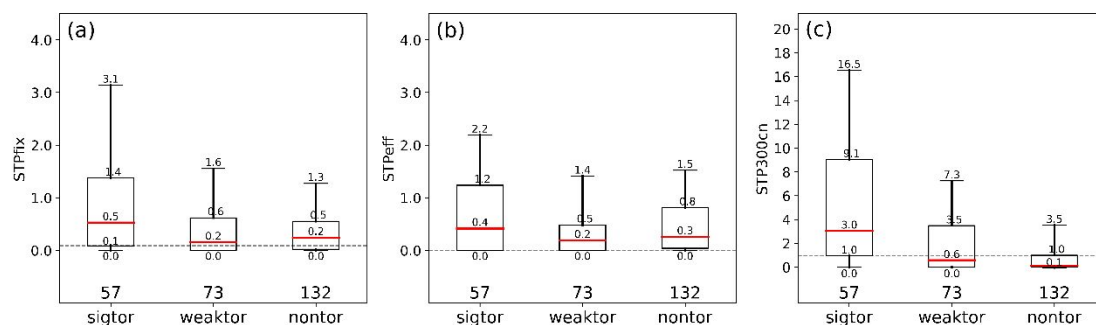


Figure 6. Composite hodographs are presented for (a) significantly tornadic supercells (sigtor; 57 cases), (b) weakly tornadic supercells (weaktor; 73 cases), and (c) nontornadic supercells (nontor; 144 cases) before (dashed black) and after (solid red) realignment of the 0–6-km shear vector. The curves are labeled with heights above ground level (AGL) in kilometers. The wind speed unit is meters per second.

4. Improvements to the STP in China

a. The current STP

The STP effectively distinguishes between tornadic and nontornadic supercells in the United States. A higher STP indicates a greater likelihood of tornado occurrence. In this section, we first examine whether STP, represented by two expressions in Eqs. (1) and (2), can also have good predictive skills for tornadic versus non-tornadic supercells in China. As shown in Figure 7a, the STP_{fix} median of nontornadic supercells calculated based on Eq. (1) is equal to that of weakly tornadic supercells, and no substantial differences are observed in their STP_{fix} distributions. The 25th percentile of STP_{fix} for significantly tornadic supercells cannot match the 75th percentile of STP_{fix} for nontornadic supercells (Figure 7a). The TSS value of STP_{fix} is 0.29 (Table 2). Therefore, the STP_{fix} as given in Eq. (1) may not be well-suited for China. The performance of STP_{eff} is even worse. The distribution of STP_{eff} for nontornadic cases is obviously higher than that for weakly tornadic supercells (Figure 7b). STP_{eff} gets a TSS value of 0.14 (Table 2). Clearly, the TSS values of STP_{fix} and STP_{eff} based on Eqs. (1) and (2) are much lower in China compared to those in the United States, where they are usually higher than 0.45 (Thompson et al., 2003, 2011). The TSS score for STP_{fix} for China overall is lower due to the significantly low score of 0.08 in the CNS region (Table 3) while that in the CNC region is relatively high at 0.51. A similar pattern is observed for STP_{eff}, and another notable low TSS value of 0.06 is found in the CNN region (Table 3).



542

Figure 7. Box-and-whisker plots of (a) STPfix, (b) STPeff, and (c) STP300cn for significantly tornadic supercells (sigtor), weakly tornadic supercells (weaktor), and nontornadic supercells (nontor). The grey dashed line represents the 25th percentile of the sigtor box for each STP. Other descriptions are as in Figure 3.

548

549

550

551

552

553

554

555

556

557

558

559

560

561

562

563

564

565

566

567

568

569

570

571

572

573

From Figures 7a and 7b, along with the TSS values of STP, we can conclude that the STP parameters as defined in Eqs. (1) and (2) are not effective in discriminating tornadic supercells, especially weakly tornadic supercells, from nontornadic supercells in China. Further insights into why STP performs poorly can be gleaned from the values of each component of STP across different storm types (Figures 8a and 8b). The thermodynamic components of STPfix calculated for the SB parcels among different storm types show similar distributions (Figure 8a). The values of the CAPE term have a slight downward trend from tornadic to nontornadic supercells (Figure 8a). The values of LCL term on the box-and-whisker are all one (maximum for the LCL term) for tornadic supercells and are below one from the 10th to the 25th percentile for nontornadic supercells (Figure 8a). Using the SRH term instead of thermodynamic terms improves the performance of discerning tornadoes, as 75% of the significantly tornadic supercells have SRH term values greater than the SRH term median for nontornadic supercells (Figure 8a). However, the distributions of SRH term are similar between weakly tornadic and nontornadic supercells (Figure 8a). The shear term of STPfix performs even worse than thermodynamic terms. The majority of shear term values for nontornadic supercells are higher than those for tornadic supercells (Figure 8a), attributed to the characteristics of SHR6 in China supercell cases.

The CAPE term of STPeff shows a similar distribution among three storm types (Figure 8b). About half of cases for each storm type have LCL term values equal to one (Figure 8b). The values of the CIN term are equal to the maximum of one for most cases (Figure 8b). Similar to the SRH term of STPfix, the SRH term of STPeff fails to differentiate between weakly tornadic and nontornadic supercells (Figure 8b). The shear term of STPeff resembles that of STPfix (Figure 8b).

574

575

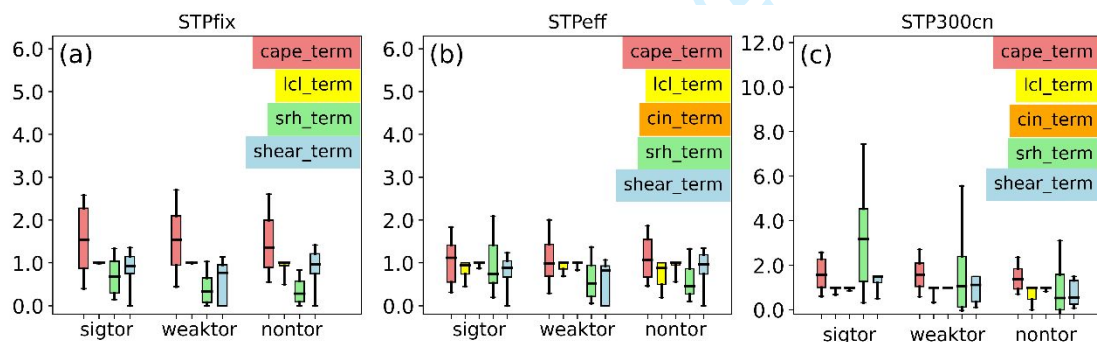
576

577

578

579

580



574

575

576

577

578

579

580

Figure 8. Box-and-whisker plots of each term in (a) STPfix, (b) STPeff, and (c) STP300cn for significantly tornadic supercells (sigtor), weakly tornadic supercells (weaktor), and nontornadic supercells (nontor). Other descriptions are as in Figure 3.

581 *b. Calibrating STP for China*

582

583

584

585

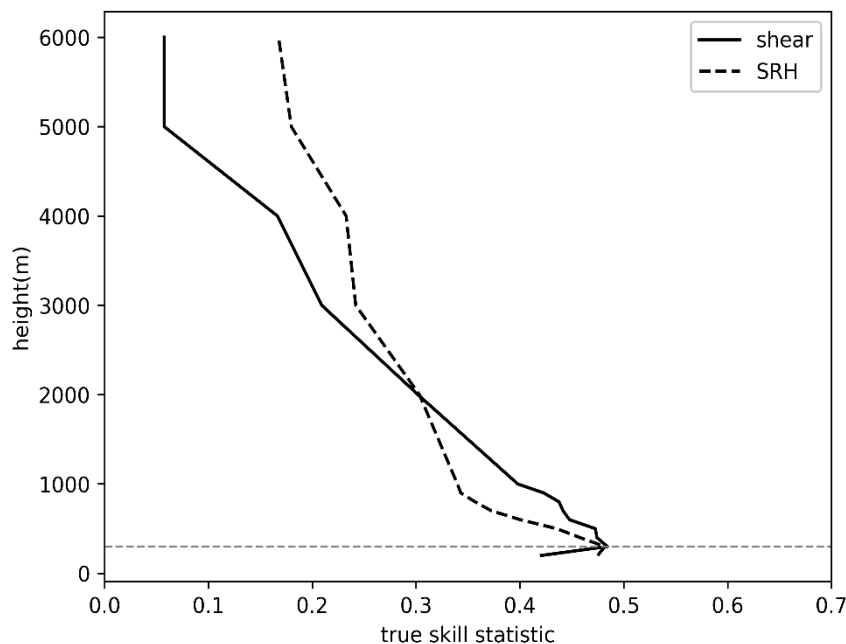
586

587

588

582 Due to the limited skill of the original formulations of STP parameters in forecasting
 583 tornadoes in China, the thermodynamic and kinematic terms in STP are calibrated based
 584 on their characteristics. When evaluating the performance of CAPE and LCL for
 585 different types of lifted parcels, the SB and MU parcels tend to exhibit better predictive
 586 skills compared to the ML parcel type. In fact, the differences between SB-based and
 587 MU-based parameters are minimal, as most of the cases used in this paper are surface-
 588 based. In this case, we choose to use CAPE, LCL, and CIN based on MU parcels in the
 589 revised STP formulation, as they are more effective for elevated storms.

590 As previously shown, the use of shallow-layer SRH and shallow-layer wind shear
 591 results in better performance. Replacing the deep-layer SRH and shear with shallow-
 592 layer SRH and shear in STP could potentially improve tornado forecasting in China.
 593 We examine the TSS values of SRH and wind shear when the top of the SRH integration
 594 and the shear layer increases from 200 m to 6000 m AGL, respectively (Figure 9). Our
 595 results demonstrate an increasing trend of TSS as the layer top height decreases for both
 596 SRH and shear. Consistent with previous studies (Coffer et al., 2019, 2020), the shallow
 597 layer of SRH indeed has a higher TSS value. Among the tested shallow-layer depths of
 598 SRH, SRH over 0-300 m depth or SRH300 exhibits the best forecasting skill. Similarly,
 599 the 0-300 m shear, SHR300, also has the highest skill among tested wind shear over
 600 various depths. The kinematic components of STP are therefore replaced with
 601 parameters based on the fixed 0-300 m depth.
 602



603
 604
 605 **Figure 9.** True skill statistic (TSS) at the optimal threshold for various
 606 depths of SRH (dashed line) and shear (solid line) integrated from 200 m to
 607 6000 m (i.e., 200 m, 300 m, 400 m, 500 m, 600 m, 700 m, 800 m, 900 m, 1000
 608 m, 2000 m, 3000 m, 4000 m, 5000 m, and 6000 m) above ground level (AGL)
 609 for discriminating between significantly tornadic and nontornadic supercells.
 610 The dashed grey line denotes the corresponding layer of the max TSS for
 611 SRH and shear. TSS is calculated at 1000 evenly spaced thresholds of the
 612 entire ERA5 sounding dataset for each layer of SRH and shear.
 613

614 To further enhance the predictive skill of the revised STP for tornadoes in China,
 615 we made several adjustments to the STP formulation. Firstly, as indicated earlier, we

used MU-based thermodynamic parameters and kinematic parameters over a fixed depth of 300 m. Additionally, to preserve the threshold of 1 for STP, the normalization denominators of some terms are adjusted. It is worth noting that modifying the denominator will not affect the maximum TSS value of each term in STP, but it does impact the optimal threshold for each term. With these changes, the formulation of the calibrated STP, which we call STP300cn, is given by

$$\text{STP300cn} = \left(\frac{\text{MUCAPE}}{2000 \text{ J kg}^{-1}} \right) \times \left(\frac{\text{MUCIN}+200}{150 \text{ J kg}^{-1}} \right) \times \left(\frac{1600-\text{MULCL}}{600 \text{ m}} \right) \times \left(\frac{\text{SRH300}}{12 \text{ m}^2\text{s}^{-2}} \right) \times \left(\frac{\text{SHR300}}{1.9 \text{ m s}^{-1}} \right) \quad (4)$$

Here are the calculation rules we apply to different terms in STP300cn. Same as the original STP, the MUCIN term is 0.0 when MUCIN is less than -150 J kg^{-1} and is 1.0 when MUCIN exceeds -50 J kg^{-1} . Given the MULCL and SHR300 distributions for supercells in China, we make adjustments to the MULCL and SHR terms. The MULCL term is set to 0 when MULCL is greater than 1600 m and is set to 1 when MULCL is less than 1000 m. The SHR300 term equals 1.5 when SHR300 is greater than 2.85 m s^{-1} and there is no lower bound. Besides, the MUCAPE and SRH300 terms still have no upper bounds and their normalizing denominators have been changed to 2000 J kg^{-1} and $12 \text{ m}^2\text{s}^{-2}$, respectively.

With the above calibrations, the TSS value of STP300cn is increased to 0.51 for the China cases, which is more than twice those of the original STPfix and STPeff (Table 2). Compared with the original STPs, STP300cn can much better distinguish between significantly tornadic and nontornadic supercells in China, which is evident from the box-and-whisker plot in Figure 7. The forecasting ability of STP300cn is further evidenced by comparing the position of the grey dashed line representing the 25th percentile value of STP for significantly tornadic supercells across all subfigures in Figure 7. Unlike the 25th percentile values of STPfix and STPeff, which are similar for significantly tornadic and nontornadic supercells (Figures 7a and 7b), the 25th percentile of STP300cn for significantly tornadic supercells matches the 75th percentile for nontornadic ones (Figure 7c). STP300cn also exhibits a markedly higher distribution for weakly tornadic supercells than for nontornadic supercells (Figure 7c).

The performance of STP300cn also varies across the three subregions in China. According to Table 3, STP300cn in CNC has the highest forecast skill with a TSS value of 0.66. This is primarily due to the impressive skills of SRH300, SHR300 and LCL in CNC. Meanwhile, STP300cn in both CNN and CNS regions achieve lower values (~ 0.4 ; Table 3) compared to the CNC region. As discussed in Section 3a, significant tornadoes in the CNN region are primarily driven by favorable kinematic conditions rather than favorable thermodynamic conditions. The lower TSS values of thermodynamic parameters result in a relatively low TSS value of STP300cn compared to that in the CNC region. Therefore, when predicting significant tornadoes in the CNN region, attention should also be paid to the individual kinematic parameters in addition to STP300cn. In the CNS region, the abundant moisture, along with relatively weak wind shear and lower horizontal streamwise vorticity, contributes to the lower TSS values of LCL and the kinematic terms in STP300cn. Still, in the CNN and CNS regions, the performance of STP300cn is much superior to those of the original STP parameters.

STP300cn also performs better than the original STPs in distinguishing between weakly tornadic and nontornadic supercells in each region (Table S1 in the Supplementary information), and the overall performance characteristics of the parameters across three regions are similar to those in distinguishing significantly tornadic and nontornadic supercells.

1
2
3 665 Although the superior performance of kinematic parameters over thermodynamic
4 666 parameters has been discussed in section 3, the performance of each component in
5 667 STP300cn is examined further in this subsection. With a TSS value of 0.05 (Table 2),
6 668 MUCIN exhibits the poorest performance among the thermodynamic components in
7 669 STP300cn. On the other hand, the forecasting skills of MUCAPE and MULCL show
8 670 improvement compared to MUCIN ($TSS_{MUCAPE}=0.18$, $TSS_{MULCL}=0.29$; Table 2). The
9 671 median of MUCAPE for significantly tornadic cases increases by about 11% compared
10 672 to that for nontornadic cases (Figure 3d). Additionally, the MULCL median increases
11 673 by nearly 31% from significantly tornadic cases to nontornadic cases (Figure 3e).
12 674 However, the distributions of the CAPE and LCL terms among the three types of
13 675 supercells are still highly overlapped (Figure 8c). Therefore, the thermodynamic
14 676 parameters in STP300cn still do not perform well by themselves, and their low skills in
15 677 CNN contribute negatively to the overall score over China.

16 678 With an optimal threshold of $10.4 \text{ m}^2\text{s}^{-2}$, SRH300 has a higher TSS value of 0.48
17 679 compared to SRH1 of 0.34 or ESRH of 0.29 (Table 2). Similarly, SHR300 has a much
18 680 higher TSS value of 0.48 compared to SHR6 of 0.06 or EBWD of 0.01 (Table 2). Not
19 681 surprisingly, the kinematic terms in STP300cn exhibit better performance when
20 682 compared to the kinematic terms in the original STP. Especially, the 25th percentile of
21 683 the SRH300 term for significantly tornadic cases closely matches the median SRH300
22 684 term for weakly tornadic cases and the 75th percentile of the SRH300 term for
23 685 nontornadic cases (Figure 8c).

24 686 Figure 10 is a performance diagram that displays additional skill metrics, including
25 687 success ratio ($1 - FAR$), POD, bias B , and critical success index (CSI) for each term in
26 688 STP300cn (Roebber, 2009). The kinematic terms at the optimal TSS values perform
27 689 better, with CSI values of about 0.45. However, they show a tendency to over-forecast,
28 690 as indicated by the high biases, particularly for SRH300. MUCAPE at the optimal TSS
29 691 shows nearly no bias but a much lower CSI value of ~ 0.25 . In contrast, MUCIN at the
30 692 optimal TSS has significant over-forecast, corresponding to a high POD value and a
31 693 low success ratio. MULCL achieves the highest CSI values among thermodynamic
32 694 terms, although it is also somewhat overforecasted.
33 695

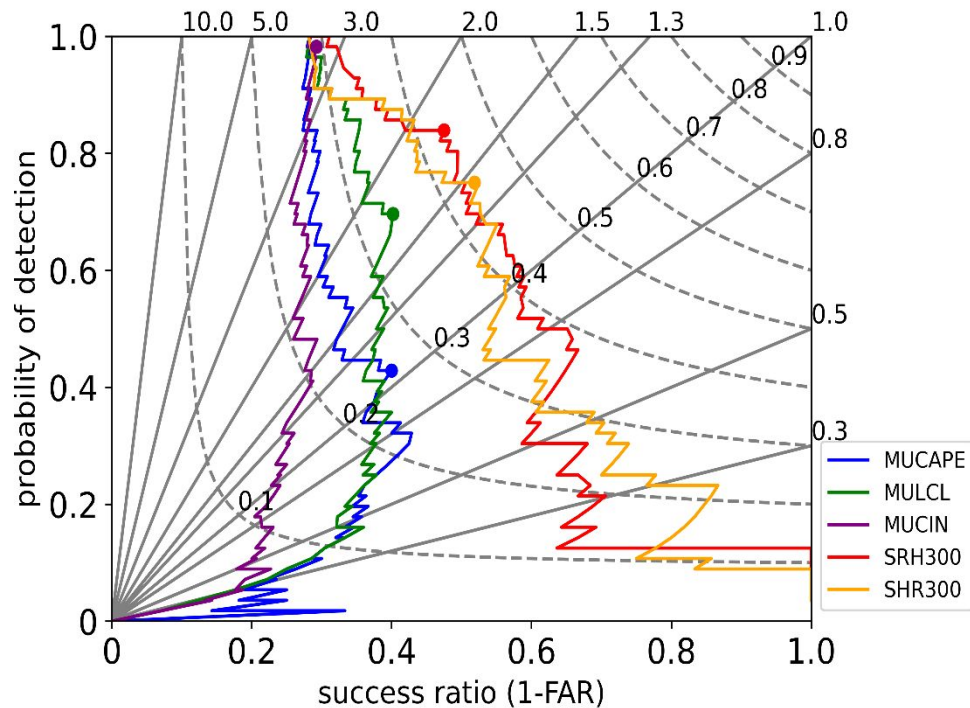


Figure 10. Performance diagram summarizing the success ratio [1 - FAR (false alarm ratio)], probability of detection, bias, and critical success index at 1000 evenly distributed thresholds of the entire ERA5 sounding dataset for each term in STP300cn, which includes the MUCAPE, MULCL, MUCIN, SRH300, and SHR300 terms. Each curve starts with a probability of detection of 1, and as the threshold increases, it shows a decrease in probability of detection. The dot on each curve indicates the threshold with the optimal TSS value. Bias scores are shown as sloping solid lines with labels on the outward extension, and the labeled dashed contours are CSI. The diagonal straight line indicates no bias and the top right corner indicates perfect CSI.

5. Discussion

In addition to assessing STP, we also investigated the efficacy of other combined parameters. BRN [$BRN = MLCAPE / 0.5(u_{avg})^2$] has served as a predictor for supercells since it was initially explored through numerical simulations (Weisman & Klemp, 1982). Environments with $BRN < 50$ are conducive to supercell formation, while environments with $BRN > 50$ favor multicellular events. With a similar BRN mean value for significantly tornadic and nontornadic supercells (Figure 4), BRN achieves the lowest TSS value of 0.07 (Table 2) among combined parameters. Another combined parameter, EHI, is developed to better determine the potential for supercells and tornadoes in a given environment (Hart & Korotky, 1991). The TSS value for 0–1-km EHI [$EHI = (CAPE)(SRH1/160000)$] is the same as that for STPfix, which is 0.26 (Table 2). Generally, most strong tornadoes occur with EHI values of 3.0–3.9 (Davies, 1993), but the mean values of EHI for significantly tornadic cases is 0.7 and for nontornadic cases is 0.4 in China (Figure 4). $VGP = [S(CAPE)^{1/2}]$, where S represents the 0–4-km mean shear, is derived from the physical concept of tilting of vorticity (Rasmussen & Blanchard, 1998). Similarly, VGP has a low TSS value of 0.17 (Table 2). $SCP [SCP = (MUCAPE/1000 \text{ J kg}^{-1})(ESRH/50 \text{ m}^2 \text{ s}^{-2})(EBWD/20 \text{ m s}^{-1})]$,

727 which has been formulated to identify environments that support supercells (Thompson
728 et al., 2003), also has a low TSS value of 0.18 (Table 2).

729 To sum up, the TSS values of the combined parameters above are all less than 0.3.
730 This is not surprising, as they are combinations of CAPE and deep-layer shear. CAPE
731 and deep-layer shear may not correlate directly with the formation of the low-level
732 mesocyclone (Brooks et al., 1994). On the contrary, the shallow-layer shear and SRH,
733 as well as useful thermodynamic parameters should be paid closer attention in China.

734 The TSS value of STP300cn ($TSS_{STP300cn}=0.51$; Table 2) is only slightly higher than
735 the TSS values for individual kinematic parameters ($TSS_{SRH300}=TSS_{SHR300}=0.48$; Table
736 2), indicating that thermodynamic terms in STP300cn only make small contributions.
737 Future research should focus on identifying and incorporating more effective
738 thermodynamic parameters into combined parameters. This entails a comprehensive
739 exploration of various atmospheric thermodynamic properties to ascertain their
740 significance in enhancing the predictive capability of combined parameters for
741 distinguishing between tornadic and nontornadic supercells.

742 Coffey et al. (2020) obtained a significant enhancement in the discrimination
743 between tornadic and nontornadic supercells through the utilization of the 0–100 m
744 AGL layer SRH. This suggests that the layer with the best predictive skill for SRH or
745 shear in China may need further exploration. Higher vertical resolution observations
746 and model output data are needed to further assess the performance of shallow-layer
747 SRH and shear for supercell environments in China, which should be helpful for
748 obtaining more reliable and insightful conclusions.

749 This paper primarily focuses on the environmental characteristics that distinguish
750 tornadic supercells from nontornadic supercells in China. Future research could utilize
751 soundings from both tornadic and nontornadic supercells in China to conduct idealized
752 simulations aimed at investigating how processes beyond environmental factors
753 contribute to tornado formation. Such studies could help identify additional influences,
754 such as storm dynamics or mesoscale interactions, that may play critical roles in tornado
755 genesis, providing a more comprehensive understanding of the factors involved in
756 tornado occurrence.

757 6. Summary and conclusions

758 In this paper, we seek to compare the environmental characteristics of tornadic and
759 nontornadic supercells in China. The ERA5 dataset that has higher spatial and temporal
760 resolutions compared to other global reanalysis datasets is used to extract proximity
761 soundings and calculate environmental parameters. A sample of 130 tornadic supercells
762 and 143 nontornadic supercells from 2002 to 2021 is used. Supercells are categorized
763 as significantly tornadic (sigtor, those rated EF2-EF4), weakly tornadic (weaktor, those
764 rated EF1) and nontornadic (nontor). Tornadic supercells are primarily concentrated in
765 the eastern regions of China, while nontornadic supercells are more widely distributed.
766 In addition to their prevalence in eastern China, nontornadic supercells also extend into
767 central regions. Tornadic supercells have a similar diurnal distribution to nontornadic
768 supercells. However, with tornadic supercells peaking in July and nontornadic
769 supercells peaking in April, their seasonal distributions are different. To explore the
770 regional characteristics, China is divided into Northern China (CNN), Central China
771 (CNC), and Southern China (CNS). True Skill Score (TSS) is used to identify the
772 environmental parameters that are effective in distinguishing between significantly
773 tornadic and nontornadic supercells.

774 Firstly, we examined thermodynamic parameters including CAPE, LCL, and CIN,
775 based on mixed-layer (ML), surface-based (SB), and most unstable (MU) lift parcels.

1
2
3 776 Additionally, kinematic parameters including SRH300, SRH1, ESRH, SHR300,
4 777 EBWD, and SHR6 were analyzed. With the median of CAPE for significantly tornadic
5 778 supercells being either less than or similar to that for weakly tornadic supercells, and
6 779 only slightly greater than that for nontornadic supercells, CAPE exhibits limited
7 780 forecasting skill (TSS less than 0.2). CAPE based on SB or MU parcels performs better.
8 781 Weakly tornadic supercells have the lowest LCL median and nontornadic supercells
9 782 have the highest LCL median. TSS values of LCL are less than 0.3. CIN (with TSS
10 783 similar to 0.1) shows even worse performance than CAPE and LCL. The low
11 784 performance of these thermodynamic parameters in China is partly related to the very
12 785 low skill in the CNN region and the worse performance of LCL in the CNS region.
13 786 Thermodynamic parameters in CNC perform better. We also examined other
14 787 thermodynamic parameters like lowRH, LR85, LR75 and LFC. There are no large
15 788 distinctions of these parameters across various storm types.

16 789 SHR6 and EBWD of nontornadic supercells are higher than those of weakly
17 790 tornadic supercells, and TSS values of SHR6 and EBWD are both less than 0.1.
18 791 SRH300 and SHR300 show the best forecast skill among SRH and shear evaluated over
19 792 other depths. The TSS values of SRH300 and SHR300 perform best in the CNC region
20 793 (~0.6) while also exhibiting a notable score of approximately 0.5 in the CNN region.
21 794 However, in the CNS region, both parameters show relatively low TSS values
22 795 (SRH~0.3 and SHR~0.4). Moreover, SRH300 and SHR300 of weakly tornadic
23 796 supercells are obviously higher than those of nontornadic supercells.

24 797 Further, we examined whether the original STP parameters (STP_{fix} and STP_{eff})
25 798 can effectively discriminate tornadic supercells from nontornadic supercells in China.
26 799 The results reveal that both STP_{fix} and STP_{eff} based on the original formulations that
27 800 were calibrated for the United States cases have limited skill (TSS_{STP_{fix}}=0.29 and
28 801 TSS_{STP_{eff}}=0.14) for the China cases, and their distributions fail to effectively distinguish
29 802 weakly tornadic from nontornadic supercells. To improve the performance, we
30 803 composed a new STP formulation by using MUCAPE, MULCL, MUCIN, SRH300,
31 804 and SHR300, to obtain a parameter we call STP300cn. The TSS value of STP300cn is
32 805 0.51, significantly higher than those of STP_{fix} and STP_{eff}. Regional differences also
33 806 exist in STP300cn. It exhibits a great performance in CNC (TSS=0.66), CNS
34 807 (TSS=0.42) and a TSS value of 0.37 in CNN, which are all much higher than TSS
35 808 values achieved by the original STPs. Moreover, the performance of each term in
36 809 STP300cn is compared in this paper. Kinematic terms (SRH300 and SHR300)
37 810 outperform thermodynamic terms (MUCAPE, MULCL, and MUCIN), though they
38 811 tend to be slightly over-forecasted. Among thermodynamic terms, MUCIN has the
39 812 worst forecast skill.

40 813 This study is limited by the relatively small sample size of tornadic and non-tornadic
41 814 supercell cases in China, as well as notable differences in their spatial and temporal
42 815 distributions. Additionally, there may be potential inaccuracies in the extracted
43 816 environmental soundings from the ERA5 dataset. Further studies should try to include
44 817 additional cases and use more accurate regional reanalysis or incorporate observed
45 818 soundings when they are available.

46 819
47 820 *Acknowledgments.* This work was primarily supported by NSFC grant 41730965.

48 821
49 822 *Data Availability Statement.* The ERA5 reanalysis dataset can be downloaded online
50 823 (<https://cds.climate.copernicus.eu/>). The software used in this paper is available online

824 (<https://github.com/sharppy/SHARPPy>). The list of tornadic and nontornadic supercells
 825 used in this paper and the related codes can be accessed at
 826 <https://doi.org/10.7910/DVN/OH0VKD>.

827

828

REFERENCES

- 829 Bai, L. (2021) Environmental analysis on the first documented tornado outbreak in
 830 China. *Atmospheric Science Letters*, **22**, e1057, <https://doi.org/10.1002/asl.1057>.
 831 Beebe, R. G. (1958) Tornado proximity soundings. *Bulletin of the American*
 832 *Meteorological Society*, **39**, 195–201, <https://doi.org/10.1175/1520-0477-39.4.195>.
 833 Blumberg, W. G., Halbert, K. T., Supinie, T. A., Marsh, P. T., Thompson, R. L. & Hart,
 834 J. A. (2017) SHARPPy: An open-source sounding analysis toolkit for the
 835 atmospheric sciences. *Bulletin of the American Meteorological Society*, **98**, 1625–
 836 1636, <https://doi.org/10.1175/BAMS-D-15-00309.1>.
 837 Brooks, H. E., Doswell III, C. A. & Cooper, J. (1994) On the environments of tornadic
 838 and nontornadic mesocyclones. *Weather and Forecasting*, **9**, 606–618,
 839 [https://doi.org/10.1175/1520-0434\(1994\)009<0606:OTEOTA>2.0.CO;2](https://doi.org/10.1175/1520-0434(1994)009<0606:OTEOTA>2.0.CO;2).
 840 Brooks, H. E., Lee, J. W. & Craven, J. P. (2003) The spatial distribution of severe
 841 thunderstorm and tornado environments from global reanalysis data. *Atmospheric*
 842 *Research*, **67–68**, 73–94, [https://doi.org/10.1016/S0169-8095\(03\)00045-0](https://doi.org/10.1016/S0169-8095(03)00045-0).
 843 China Meteorological Administration. (2005–2022) *Yearbook of Meteorological*
 844 *Disasters in China* (in Chinese). Meteorological Press.
 845 Coffey, B. & Parker, M. D. (2015) Impacts of increasing low-level shear on supercells
 846 during the early evening transition. *Monthly Weather Review*, **143**, 1945–1969,
 847 <https://doi.org/10.1175/MWR-D-14-00328.1>.
 848 Coffey, B. & Parker, M. D. (2017) Simulated supercells in nontornadic and tornadic
 849 VORTEX2 environments. *Monthly Weather Review*, **145**, 149–180,
 850 <https://doi.org/10.1175/MWR-D-16-0226.1>.
 851 Coffey, B., Parker, M. D., Dahl, J. M. L., Wicker, L. J. & Clark, A. J. (2017) Volatility
 852 of tornadogenesis: an ensemble of simulated nontornadic and tornadic supercells in
 853 VORTEX2 environments. *Monthly Weather Review*, **145**, 4605–4625,
 854 <https://doi.org/10.1175/MWR-D-17-0152.1>.
 855 Coffey, B. & Parker, M. D. (2018) Is there a “tipping point” between simulated
 856 nontornadic and tornadic supercells in VORTEX2 environments? *Monthly Weather*
 857 *Review*, **146**, 2667–2693, <https://doi.org/10.1175/MWR-D-18-0050.1>.
 858 Coffey, B., Parker, M. D., Thompson, R. L., Smith, B. T. & Jewell, R. E. (2019) Using
 859 near-ground storm relative helicity in supercell tornado forecasting. *Weather and*
 860 *Forecasting*, **34**, 1417–1435, <https://doi.org/10.1175/WAF-D-19-0115.1>.
 861 Coffey, B., Taszarek, M. & Parker, M. D. (2020) Near-ground wind profiles of tornadic
 862 and nontornadic environments in the United States and Europe from ERA5
 863 reanalyses. *Weather and Forecasting*, **35**, 2621–2638,
 864 <https://doi.org/10.1175/WAF-D-20-0153.1>.
 865 Craven, J. P. & Brooks, H. E. (2004) Baseline climatology of sounding derived
 866 parameters associated with deep, moist convection. *National Weather Digest*,
 867 **28**, 13–24,
 868 https://www.nssl.noaa.gov/users/brooks/public_html/papers/cravenbrooksna.pdf
 869 .

- 1
2
3 870 Davies, J. M. (1993) Hourly helicity, instability, and EHI in forecasting supercell
4 871 tornadoes. Preprints, *17th Conference on Severe Local Storms*, Kansas City, MO,
5 872 American Meteorological Society, 107–111.
- 6 873 Davies, J. M. (2004) Estimations of CIN and LFC associated with tornadic and
7 874 nontornadic supercells. *Weather and Forecasting*, **19**, 714–726,
8 875 [https://doi.org/10.1175/1520-0434\(2004\)019<0714:EOCALA>2.0.CO;2](https://doi.org/10.1175/1520-0434(2004)019<0714:EOCALA>2.0.CO;2).
- 9 876 Davies-Jones, R. (1984) Streamwise vorticity: The origin of updraft rotation in
10 877 supercell storms. *Journal of the Atmospheric Sciences*, **41**, 2991–3006,
11 878 [https://doi.org/10.1175/1520-0469\(1984\)041<2991:SVTOOU>2.0.CO;2](https://doi.org/10.1175/1520-0469(1984)041<2991:SVTOOU>2.0.CO;2).
- 12 879 Davies-Jones, R. P., Burgess, D. & Foster, M. (1990) Test of helicity as a forecast
13 880 parameter. Preprints, *16th Conference on Severe Local Storms*, Kananaskis Park,
14 881 AB, Canada, American Meteorological Society, 588–592.
- 15 882 Davies-Jones, R. (2015) A review of supercell and tornado dynamics. *Atmospheric*
16 883 *Research*, **158–159**, 274–291, <https://doi.org/10.1016/j.atmosres.2014.04.007>.
- 17 884 Ding, Y. (2008) *The Collection of Meteorological Disasters Records in China* (in
18 885 Chinese). Meteorological Press, pp. 948.
- 19 886 Donaldson, R. J. & Desrochers, P. R. (1990) Improvement of tornado warnings by
20 887 Doppler radar measurement of mesocyclone rotational kinetic energy. *Weather and*
21 888 *Forecasting*, **5**, 247–258.
- 22 889 Doswell, C. A., Davies-Jones, R. & Keller, D. L. (1990) On summary measures of skill
23 890 in rare event forecasting based on contingency tables. *Weather and Forecasting*, **5**,
24 891 576–585, [https://doi.org/10.1175/1520-0434\(1990\)005<0576:OSMOSI>2.0.CO;2](https://doi.org/10.1175/1520-0434(1990)005<0576:OSMOSI>2.0.CO;2).
- 25 892 Doswell, C. A. & Flueck, J. A. (1989) Forecasting and verifying in a field research
26 893 project: DOPLIGHT '87. *Weather and Forecasting*, **4**, 97–109,
27 894 [https://doi.org/10.1175/1520-0434\(1989\)004<0097:FAVIAF>2.0.CO;2](https://doi.org/10.1175/1520-0434(1989)004<0097:FAVIAF>2.0.CO;2).
- 28 895 Doswell, C. A. & Evans, J. S. (2003) Proximity sounding analysis for derechos and
29 896 supercells: An assessment of similarities and differences. *Atmospheric Research*,
30 897 **67–68**, 117–133, [https://doi.org/10.1016/S0169-8095\(03\)00047-4](https://doi.org/10.1016/S0169-8095(03)00047-4).
- 31 898 Edwards, R., Dean, A. R., Thompson, R. L. & Smith, B. T. (2012) Convective modes
32 899 for significant severe thunderstorms in the contiguous United States. Part III:
33 900 Tropical cyclone tornadoes. *Weather and Forecasting*, **27**, 1507–1519,
34 901 <https://doi.org/10.1175/WAF-D-11-00117.1>.
- 35 902 Evans, J. S. & Doswell, C. A. (2001) Examination of derecho environments using
36 903 proximity soundings. *Weather and Forecasting*, **16**, 329–342,
37 904 [https://doi.org/10.1175/1520-0434\(2001\)016<0329:EODEUP>2.0.CO;2](https://doi.org/10.1175/1520-0434(2001)016<0329:EODEUP>2.0.CO;2).
- 38 905 Fawbush, E. J. & Miller, R. C. (1954) The types of air masses in which North American
39 906 tornadoes form. *Bulletin of the American Meteorological Society*, **35**, 154–165,
40 907 <https://doi.org/10.1175/1520-0477-35.4.154>.
- 41 908 Fan, W. & Yu, X. (2015) Characteristics of spatial-temporal distribution of tornadoes
42 909 in China (in Chinese with English abstract). *Meteorological Monthly*, **41**, 793–805.
43 910 <https://doi.org/10.7519/j.issn.1000-0526.2015.07.001>
- 44 911 Fischer, J. & Dahl, J. M. L. (2022) Transition of near-ground vorticity dynamics during
45 912 tornadogenesis. *Journal of the Atmospheric Sciences*, **79**, 467–483,
46 913 <https://doi.org/10.1175/JAS-D-21-0181.1>
- 47 914 Hart, J. A. & Korotky, W. (1991) The SHARP workstation v 1.50 users guide.
48 915 NOAA/NWS Document, 30 pp.
- 49 916 Hersbach, H. & Coauthors (2020) The ERA5 global reanalysis. *Quarterly Journal of*
50 917 *the Royal Meteorological Society*, **146**, 1999–2049, <https://doi.org/10.1002/qj.3803>.
- 51 918

- 1
2
3 919 Klees, A. M., Richardson, Y. P., Markowski, P. M., Weiss, C., Wurman, J. & Kosiba,
4 920 K. K. (2016) Comparison of the tornadic and nontornadic supercells intercepted by
5 921 VORTEX2 on 10 June 2010. *Monthly Weather Review*, **144**, 3201–3231,
6 922 <https://doi.org/10.1175/MWR-D-15-0345.1>.
- 7
8 923 Lemon, L. R. & Doswell, C. A. (1979) Severe thunderstorm evolution and mesocyclone
9 924 structure as related to tornadogenesis. *Monthly Weather Review*, **107**, 1184–1197,
10 925 [https://doi.org/10.1175/1520-0493\(1979\)107<1184:STEAMS>2.0.CO;2](https://doi.org/10.1175/1520-0493(1979)107<1184:STEAMS>2.0.CO;2).
- 11 926 Markowski, P. M., Straka, J. M. & Rasmussen, E. N. (1998) A preliminary investigation
12 927 of the importance of helicity location in the hodograph. *19th Conference on Severe*
13 928 *Local Storms*, Minneapolis, MN, American Meteorological Society, 230–233.
- 14 929 Markowski, P. M., Straka, J. M. & Rasmussen, E. N. (2002) Direct surface
15 930 thermodynamic observations within the rear-flank downdrafts of nontornadic and
16 931 tornadic supercells. *Monthly Weather Review*, **130**, 1692–1721,
17 932 [https://doi.org/10.1175/1520-0493\(2002\)130<1692:DSTOWT>2.0.CO;2](https://doi.org/10.1175/1520-0493(2002)130<1692:DSTOWT>2.0.CO;2).
- 18 933 Markowski, P., Hannon, C., Frame, J., Lancaster, E., Pietrycha, A., Edwards, R. &
19 934 Thompson, R. L. (2003) Characteristics of vertical wind profiles near supercells
20 935 obtained from the Rapid Update Cycle. *Weather and Forecasting*, **18**, 1262–1272,
21 936 [https://doi.org/10.1175/1520-0434\(2003\)018<1262:COVWPN>2.0.CO;2](https://doi.org/10.1175/1520-0434(2003)018<1262:COVWPN>2.0.CO;2).
- 22 937 Markowski, P. M. & Richardson, Y. (2010) *Mesoscale Meteorology in Midlatitudes*.
23 938 John Wiley & Sons, Ltd, pp. 407.
- 24 939 Markowski, P. M. & Richardson, Y. (2014) The influence of environmental low-level
25 940 shear and cold pools on tornadogenesis: Insights from idealized simulations.
26 941 *Journal of the Atmospheric Sciences*, **71**, 243–275, [https://doi.org/10.1175/JAS-D-](https://doi.org/10.1175/JAS-D-13-0159.1)
27 942 [13-0159.1](https://doi.org/10.1175/JAS-D-13-0159.1).
- 28 943 Mead, C. (1997) The discrimination between tornadic and nontornadic supercell
29 944 environments: a forecasting challenge in the southern United States. *Weather and*
30 945 *Forecasting*, **12**, 379–387, [https://doi.org/10.1175/1520-](https://doi.org/10.1175/1520-0434(1997)012<0379:TDBTAN>2.0.CO;2)
31 946 [0434\(1997\)012<0379:TDBTAN>2.0.CO;2](https://doi.org/10.1175/1520-0434(1997)012<0379:TDBTAN>2.0.CO;2).
- 32 947 Peirce, C. S. (1884) The numerical measure of the success of predictions. *Science*, **4**,
33 948 453–454, <https://doi.org/10.1126/science.ns-4.93.453-a>.
- 34 949 Rasmussen, E. N. & Blanchard, D. O. (1998) A baseline climatology of sounding-
35 950 derived supercell and tornado forecast parameters. *Weather and Forecasting*, **13**,
36 951 1148–1164, [https://doi.org/10.1175/1520-](https://doi.org/10.1175/1520-0434(1998)013,1148:ABCOSD.2.0.CO;2)
37 952 [0434\(1998\)013,1148:ABCOSD.2.0.CO;2](https://doi.org/10.1175/1520-0434(1998)013,1148:ABCOSD.2.0.CO;2).
- 38 953 Roebber, P. J. (2009) Visualizing multiple measures of forecast quality. *Weather and*
39 954 *Forecasting*, **24**, 601–608, <https://doi.org/10.1175/2008WAF2222159.1>.
- 40 955 Rotunno, R., Markowski, P. M. & Bryan, G. H. (2017) “Near ground” vertical vorticity
41 956 in supercell thunderstorm models. *Journal of the Atmospheric Sciences*, **74**, 1757–
42 957 1766, <https://doi.org/10.1175/JAS-D-16-0288.1>.
- 43 958 Schenkman, A. D., Xue, M. & Hu, M. (2014) Tornadogenesis in a high-resolution
44 959 simulation of the 8 May 2003 Oklahoma City supercell. *Journal of the Atmospheric*
45 960 *Sciences*, **71**, 130–154, <https://doi.org/10.1175/JAS-D-13-073.1>.
- 46 961 Showalter, A. K. & Fulks, J. R. (1943) Preliminary report on tornadoes. U.S. Weather
47 962 Bureau, 162 pp.
- 48 963 Stensrud, D. J., Cortinas, J. & Brooks, H. E. (1997) Discriminating between tornadic
49 964 and nontornadic thunderstorms using mesoscale model output. *Weather and*
50 965 *Forecasting*, **12**, 613–632, [https://doi.org/10.1175/1520-](https://doi.org/10.1175/1520-0434(1997)012<0613:DBTANT>2.0.CO;2)
51 966 [0434\(1997\)012<0613:DBTANT>2.0.CO;2](https://doi.org/10.1175/1520-0434(1997)012<0613:DBTANT>2.0.CO;2).
- 52 967 Taszarek, M., Allen, J. T., Púčik, T., Hoogewind, K. A. & Brooks, H. E. (2020) Severe
53 968 convective storms across Europe and the United States. Part II: ERA5 environments

- 1
2
3 969 associated with lightning, large hail, severe wind, and tornadoes. *Journal of*
4 970 *Climate*, **33**, 10263–10286, <https://doi.org/10.1175/JCLI-D-20-0346.1>.
- 5
6 971 Thompson, R. L. (1998) Eta model storm-relative winds associated with tornadic and
7 972 nontornadic supercells. *Weather and Forecasting*, **13**, 125–137,
8 973 [https://doi.org/10.1175/1520-0434\(1998\)013<0125:EMSRWA>2.0.CO;2](https://doi.org/10.1175/1520-0434(1998)013<0125:EMSRWA>2.0.CO;2).
- 9
10 974 Thompson, R. L., Edwards, R., Hart, J. A., Elmore, K. L. & Markowski, P. M. (2003)
11 975 Close proximity soundings within supercell environments obtained from the rapid
12 976 update cycle. *Weather and Forecasting*, **18**, 1243–1261,
13 977 [https://doi.org/10.1175/1520-0434\(2003\)018<1243:CPSWSE>2.0.CO;2](https://doi.org/10.1175/1520-0434(2003)018<1243:CPSWSE>2.0.CO;2).
- 14
15 978 Thompson, R. L., Edwards, R. & Mead, C. M. (2011) An update to the supercell
16 979 composite and significant tornado parameters. *22nd Conference on Severe Local*
17 980 *Storms*, Norman, OK, American Meteorological Society, P8.1,
18 981 <http://ams.confex.com/ams/pdfpapers/82100.pdf>.
- 19
20 982 Thompson, R. L., Mead, C. M. & Edwards, R. (2007) Effective storm-relative helicity
21 983 and bulk shear in supercell thunderstorm environments. *Weather and Forecasting*,
22 984 **22**, 102–115, <https://doi.org/10.1175/WAF969.1>.
- 23
24 985 Trapp, R. J. (1999) Observations of nontornadic low-level mesocyclones and attendant
25 986 tornadogenesis failure during VORTEX. *Monthly Weather Review*, **127**, 1693–
26 987 1705, [https://doi.org/10.1175/1520-0493\(1999\)127<1693:OONLLM>2.0.CO;2](https://doi.org/10.1175/1520-0493(1999)127<1693:OONLLM>2.0.CO;2).
- 27
28 988 Veloso-Aguila, D., Rasmussen, K. L. & Maloney, E. D. (2023) Tornadoes in southeast
29 989 south America: mesoscale to planetary-scale environments. *Monthly Weather*
30 990 *Review*, **152**, 295–318, <https://doi.org/10.1175/MWR-D-22-0248.1>.
- 31
32 991 Wakimoto, R. M. & Cai, H. (2000) Analysis of a nontornadic storm during VORTEX
33 992 95. *Monthly Weather Review*, **128**, 565–592, [http://doi.org/10.1175/1520-](http://doi.org/10.1175/1520-0493(2000)128,0565:AOANSD.2.0.CO;2)
34 993 [0493\(2000\)128,0565:AOANSD.2.0.CO;2](http://doi.org/10.1175/1520-0493(2000)128,0565:AOANSD.2.0.CO;2).
- 35
36 994 Wakimoto, R. M., Cai, H. & Murphey, H. V. (2004) The Superior, Nebraska, supercell
37 995 during BAMEX. *Bulletin of the American Meteorological Society*, **85**, 1095–1106,
38 996 <http://doi.org/10.1175/BAMS-85-8-1095>.
- 39
40 997 Wang, X., Yu, X. & Zhou, X. (2015) Study of Northeast China tornadoes: The
41 998 environmental characteristics (in Chinese with English abstract). *Acta*
42 999 *Meteorologica Sinica*, **73**, 425–441.
- 43
44 1000 Weisman, M. L. (1996) On the use of vertical wind shear versus helicity in interpreting
45 1001 supercell dynamics. Preprints, *18th Conference on Severe Local Storms*, San
46 1002 Francisco, CA, American Meteorological Society, 200–204.
- 47
48 1003 Weisman, M. L. & Klemp, J. B. (1982) The dependence of numerically simulated
49 1004 convective storms on vertical wind shear and buoyancy. *Monthly Weather Review*,
50 1005 **110**, 504–520, [https://doi.org/10.1175/1520-](https://doi.org/10.1175/1520-0493(1982)110<0504:TDONSC>2.0.CO;2)
51 1006 [0493\(1982\)110<0504:TDONSC>2.0.CO;2](https://doi.org/10.1175/1520-0493(1982)110<0504:TDONSC>2.0.CO;2).
- 52
53 1007 Weisman, M. L. & Klemp, J. B. (1984) The structure and classification of numerically
54 1008 simulated convective storms in directionally varying wind shears. *Monthly Weather*
55 1009 *Review*, **112**, 2479–2498, [https://doi.org/10.1175/1520-](https://doi.org/10.1175/1520-0493(1984)112<2479:TSACON>2.0.CO;2)
56 1010 [0493\(1984\)112<2479:TSACON>2.0.CO;2](https://doi.org/10.1175/1520-0493(1984)112<2479:TSACON>2.0.CO;2).
- 57
58 1011 Weisman, M. L. & Klemp, J. B. (1986) Characteristics of isolated convective storms.
59 1012 *Mesoscale Meteorology and Forecasting*, American Meteorological Society,
60 1013 Boston, MA, pp. 331–358, https://doi.org/10.1007/978-1-935704-20-1_15.
- 1014
1015 Wilks, D. S. (2020) *Statistical Methods in the Atmospheric Sciences*. 4rd ed. Elsevier,
1016 pp. 381.
- 1017
1018 Yu, X., Zhao, J. & Fan, W. (2021) Tornadoes in China: spatiotemporal distribution and
1019 environmental characteristics (in Chinese with English abstract). *Journal of*

- 1
2
3 1018 *Tropical Meteorology*, **37**, 681–692, [https://doi.org/10.16032/j.issn.1004-](https://doi.org/10.16032/j.issn.1004-4965.2021.064)
4 1019 [4965.2021.064](https://doi.org/10.16032/j.issn.1004-4965.2021.064).
5 1020 Zhang, C., Xue, M., Zhu, K. & Yu, X. (2023) Climatology of significant tornadoes
6 1021 within China and comparison of tornado environments between United States and
7 1022 China. *Monthly Weather Review*, **151**, 465–484, [https://doi.org/10.1175/MWR-D-](https://doi.org/10.1175/MWR-D-22-0070.1)
8 1022 [22-0070.1](https://doi.org/10.1175/MWR-D-22-0070.1).
9 1023
10 1024 Zheng, Y. (2020) Review of climatology and favorable environmental conditions of
11 1025 tornado in China (in Chinese with English abstract). *Advances in Meteorological*
12 1026 *Science and Technology*, **10**, 69–75.
13 1027 Zhou, X., Wang, X., Yu, X. & Fei, H. (2012) Application of excess rotation kinetic
14 1028 energy in distinguishing the tornadic and non-tornadic mesocyclones in China (in
15 1029 Chinese with English abstract). *Plateau Meteorology*, **31**, 137–143.
16 1030 Zhou, R., Meng, Z. & Bai, L. (2021) Differences in tornado activities and key tornadic
17 1031 environments between China and the United States. *International Journal of*
18 1031 *Climatology*, **42**, 367–384, <https://doi.org/10.1002/joc.7248>.
19 1032
20
21
22
23
24
25
26
27
28
29
30
31
32
33
34
35
36
37
38
39
40
41
42
43
44
45
46
47
48
49
50
51
52
53
54
55
56
57
58
59
60